Full Title: Plant A20/AN1 proteins coordinate different immune responses including RNAi pathway for antiviral immunity

Short Title: Plant A20/AN1 proteins coordinate RNAi-mediated antiviral immunity

Authors: Li Chang[1,2,3], Ho-Hsiung Chang[2], Yi-Shu Chiu[2], Jui-Che Chang[2], Duen-Wei Hsu[4], Yuh Tzean[2], An-Po Cheng [2], Hsiang-Chia Lu[5], and Hsin-Hung Yeh[2,5*]

Affiliations:

[1]Molecular and Biological Agricultural Sciences Program, Taiwan International Graduate Program, National Chung-Hsing University, Academia Sinica, Taiwan

[2]Agricultural Biotechnology Research Center, Academia Sinica, Taipei, Taiwan

[3]Graduate Institute of Biotechnology, National Chung-Hsng University, Taichung, Taiwan

[4]Department of Biotechnology, National Kaohsiung Normal University, Kaohsiung, Taiwan.

[5]Department of Plant Pathology and Microbiology, National Taiwan University, Taipei, Taiwan.

[*]Corresponding author:

E-mail: hyeh@sinica.edu.tw (HHY)

Abstract

Salicylic acid (SA) plays important roles in antiviral immunity; however, detailed mechanisms remain elusive. Previously we identified A20/AN1 zinc-finger domain-containing protein, orchid Pha13, and *Arabidopsis* stress associated protein 5 (AtSAP5), which function similarly and serve as a hub to regulate SA-mediated immune response for antiviral immunity. In this study, another orchid A20/AN1 protein, Pha21, which shares 69.5% amino acid sequence identity with Pha13, was analyzed. Similar to Pha13 and AtSAP5, Pha21 can be found localized in the nucleus, and confers self-E3 ligase and ubiquitin binding activities. Like *Pha13* and *AtSAP5*, *Pha21* is induced by virus infection, and confers strong antiviral immunity in both transgenic orchid and *Arabidopsis* overexpressing *Pha21*. *Pha21* is also early-induced by SA treatment, and is involved in the SA-signaling pathway downstream of SA and upstream of the expression of the orchid homolog of the master regulator *NPR1*. However, in comparison with Pha13 and AtSAP5, Pha21 plays opposite roles in the expression of two SA-induced immune responsive genes, *PhaRdR1* (orchid homolog of *RNA-dependent RNA polymerase 1*) and *PhaGRXC9* (orchid homolog of *Glutaredoxin-C9*). Expression analysis suggested that Pha13 plays a dominant role in comparison to Pha21 in the expression of *PhaRdR1* and *PhaGRXC9*; however, we found that Pha21 and AtSAP5, but not Pha13, are involved in the expression of important players in the RNAi pathway, *Dicer-like nuclease 4* (*DCL4*) and *Argonaut 1* (*AGO1*) in orchid and *Arabidopsis*, respectively. Functional domain analysis revealed that both A20 and AN1 domains of Pha21 are required for virus accumulation; the AN1 domain plays a more important role in the expression of *PhaDCL4,* and neither domain is required for the

44 expression of *PhaAGO1*. Collectively, our data suggests that plant A20/AN1 proteins,
45 which are central and conserved players among plants, coordinate several immune
46 responses including the RNAi pathway to confer antiviral immunity.
47

48 **Author summary**

49 Salicylic acid (SA)-mediated antiviral immunity plays an important role to protect
50 plants from virus infection; however, the detailed mechanisms remain elusive. We
51 previously demonstrated that two plant A20/AN1 proteins, orchid Pha13 and
52 *Arabidopsis* AtSAP5, function similarly and serve as an important hub to regulate SA-
53 mediated antiviral immunity. In this study, we identified another orchid A20/AN1
54 protein, Pha21, which is involved in SA-mediated antiviral immunity. In contrast to
55 Pha13 and AtSAP5, Pha21 plays negative roles in the expression of *PhaRdR1* (orchid
56 homolog of *RNA-dependent RNA polymerase 1*) and *PhaGRXC9* (orchid homolog of
57 *Glutaredoxin-C9*). However, Pha21 and AtSAP5, but not Pha13, are involved in the
58 expression of important players in RNAi pathway, *Dicer-like nuclease 4* (*DCL4*) and
59 *Argonaut 1* (*AGO1*) in orchid and *Arabidopsis*, respectively. Our data demonstrates that
60 plant A20/AN1 proteins are conserved players in SA-mediated antiviral resistance
61 among plants, and provide links between the A20/AN1 proteins and the RNAi pathway.

62 **Introduction**

63 The plant hormone salicylic acid (SA) is important to trigger plant immunity
64 especially against biotrophic pathogens such as viruses (1-4). In facing pathogen
65 invasion, plants recognize conserved microbe-associated molecular patterns (MAMPs)
66 by pattern-recognition receptors and trigger pathogen (or pattern)-triggered immunity

67 (PTI) as the first line of defense (5, 6). Although PTI provides protection from invasion
68 by most pathogens, some have evolved, and can utilize different effectors to suppress
69 PTI for successful infection (7). Plants have evolved resistance (R) proteins capable of
70 detecting these effectors to trigger effecter-triggered immunity (ETI) for a second line
71 of plant defense (7). ETI is generally associated with programmed cell death leading to
72 the formation of necrotic lesions, which is also known as hypersensitive response (HR)
73 to prevent the further spreading of pathogen infection (1).

74 Current evidence suggests that the PTI is important to limit virus infection (8-10),
75 and the viral double strand RNA (dsRNA) has been shown to serve as a conserved
76 MAMP (10). In addition, ETI also plays an important role in combating virus infection
77 in plants. For example, the N gene from *Nicotiana glutinosa* serves as an R protein to
78 specifically recognize the effector from *Tobacco mosaic virus* (TMV) and trigger the
79 ETI (11-14). SA plays important roles in triggering PTI and ETI (15). In addition, the
80 TMV-infected tobacco plant showing local necrotic lesions was found to become more
81 resistant against secondary virus infection in the distal leaves (16, 17). This systemic
82 immune response is known as systemic acquired resistance, which is a common plant
83 immune response and plays an important role in protecting plants from pathogen
84 infection (4).

85 In addition, RNA silencing or RNA interference (RNAi) has also been
86 demonstrated to play an important role in combating virus infection (18, 19). RNAi is
87 activated through the appearance of the viral dsRNA upon virus infection. The dsRNA
88 can be cleaved to short small-interfering dsRNA (siRNA) of 21–24 nucleotides (nt) in
89 size by the Dicer-like (DCL) nuclease (20). DCL2 and DCL4 in *Arabidopsis* play an

90 important role in generating the virus-derived siRNA (vsiRNA) (19, 21, 22). The
91 vsiRNA is further unwound and one strand (guide-strand) is incorporated into the RNA-
92 induced silencing complex (RISC) (19). This complex targets viral RNA with a
93 sequence that is complementary to the guide-strand and degrades the target RNA by
94 the catalytic component of the RISC, Argonaut (AGO) nucleases (19, 20, 23, 24).
95 Among the *Arabidopsis* AGOs, AGO1 plays an important role in the antiviral immunity
96 against RNA viruses. (24). More vsiRNA can be further generated *de novo* through the
97 cellular RNA-dependent RNA polymerases (RDRs) to trigger the secondary RNA
98 silencing against viruses (25-27). SA also plays important roles in the RNAi-pathway
99 as SA treatment can induce genes involved in the RNAi pathway including RDRs in
100 *Arabidopsis*, *Nicotiana tabacum and* Tomato , and DCL and AGO in Tomato (28-32).
101 SA induces the fluctuation of redox and serves as a signal to activate sets of
102 defense genes (33, 34). The SA-induced redox change can modify the NPR1
103 (nonexpressor of pathogenesis-related protein 1) from the multimeric protein complex
104 to a monomer via the oxidoreductases, *Thioredoxin-3* and *Thioredoxin-5* (35, 36). The
105 NPR1 monomer moves into the nucleus and activates multiple defense-related genes
106 including the *PR* (pathogenesis-related protein) gene in the SA-signaling pathway (37-
107 39). In addition to the NPR1-dependent immune pathway, some data also suggest that
108 the existence of a NPR1-independent pathway contributes to the virus resistance (40,
109 41). Despite the importance of the SA governed immune pathway in antiviral immunity,
110 the regulation of this pathway remains largely elusive.
111 Proteins containing zinc-finger A20 and/or AN1 domains play an important role
112 in plant response against various abiotic stresses, and are known as stress associated

113 protein (SAPs). SAPs are conserved among different organisms (42, 43). Different
114 numbers of SAP homologs (range from 1 to 19) have been identified in organisms
115 including protists, fungi, animals, plants, and humans (42, 43). Compared to animals,
116 more of these proteins are found in plants. So far, 18, 14 and 14 SAPs have been
117 identified in rice, *Arabidopsis*, and *Phalaenopsis* orchid, respectively (42, 44).
118 Biochemical studies of proteins containing A20 and/or AN1 domains revealed that the
119 A20 domain confers E3 ligase and ubiquitin binding activity (43-49). The A20 domain
120 of human A20, Rabex-5 (guanine nucleotide exchange factor), *Arabidopsis* AtSAP5
121 and orchid Pha13 have been reported to exhibit E3 ligase activity (44, 45, 49, 50). In
122 addition, it has been shown that the A20 domain can also bind to various ubiquitin
123 chains (44, 46-48). In contrast to the A20 domain, the biochemical function of the AN1
124 domain is not fully understood.

125 Our recent study indicates that plant SAPs play a pivotal role in SA governed
126 antiviral immunity (44). Orchid *Pha13* and *Arabidopsis AtSAP5* are induced by SA
127 treatment at the early stage, and are involved in expression of orchid or *Arabidopsis*
128 *NPR1* and *NPR1*-independent immune responsive genes including the induction of
129 plant *RdR1*. In addition to Pha13, our previous virus-induced gene silencing (VIGS)
130 assay also allowed us to identify the involvement of orchid *PhaTF21* (designated here
131 as *Pha21*) in SA–regulated immune response genes (51). Pha13 and Pha21 share 69.5%
132 amino sequence identity, and are most closely related among the orchid SAPs (44).
133 Whether Pha21 and Pha13 work in a cooperative manner in plant antiviral immunity
134 remains to be explored.

135 Here, we performed a detailed study of Pha21, and compared its biochemical and
136 physiological function to Pha13. Pha21 and Pha13 share similar biochemical properties
137 including E3-ligase and ubiquitin binding activities. Our results also indicate that
138 similar to *Pha13*, *Pha21* is early-induced by SA, involved in the expression of the
139 *PhaNPR1* and *PhaNPR1*-independent genes, and plays an important role in antiviral
140 immunity. Importantly, our studies show that Pha21 is involved in expression of orchid
141 *DCL4* and *AGO1*. Together with our previous data, these studies suggest that Pha13
142 and Pha21 coordinate the expression of genes important in the RNAi pathway including
143 orchid *RdR1*, *DCL4* and *AGO1*. In addition, our previous data and data presented in
144 this study also showed that *Arabidopsis* AtSAP5 is involved in expression of *RdR1*,
145 *DCL4* and *AGO1*. Collectively, our data indicates that plant A20/AN1 proteins
146 involved antiviral immunity are conserved among plants, and the antiviral immunity is
147 partly through the RNAi pathway. Our findings suggest that A20/AN1 proteins may
148 serve as a link between SA and the RNAi pathway at the early stage of SA induced-
149 antiviral immunity.

150 **Results**

151 **Sequence and expression pattern analysis of Pha21**

152 Previously, we reported that *Pha21* (Orchidstra 2.0 database,
153 http://orchidstra2.abrc.sinica.edu.tw, accession number PATC144963) is involved in
154 the SA induced immune pathway in *P. aphrodite* (52). Pha21 contains dual zinc-finger
155 domains, A20 and AN1, in the N-terminal and C-terminal, respectively (Fig 1), and
156 belongs to the stress associated protein (SAP) family (43). Among the SAPs of *P.*
157 *aphrodite*, Pha21 is most related to our previously reported Pha13 and shared 69.5%

158 amino acid sequence identity (44). The A20 and AN1 zinc finger domains of Pha21
159 also shared high amino acid sequence identity among SAPs from different species
160 including AtSAP5 from *Arabidopsis,* and OsSAP3 and OsSAP5 from *Oryza sativa* (Fig
161 1B). (44). Unlike Pha13, no nuclear localization signal was identified in Pha21 (Fig
162 1A).

163 The expression of *Pha21* was analyzed in different tissues of *P. aphrodite* orchid
164 including root, leaf, septal, petal, lip, and column. The results revealed that *Pha21*
165 expression was higher in the column, root and leaf (S1A Fig). In addition, we also
166 analyzed the absolute expression of *Pha21* and *Pha13* in the leaves of *P. aphrodite* by
167 use of droplet digital PCR. The results indicated that *Pha21* RNA expression is about
168 15 times lower than *Pha13* in leaves of *P. aphrodite* (S1B Fig)

169 ***Pha21* is involved in the expression of SA responsive genes, *PhaNPR1* and *PhaPR1***

170 To further analyze the role of *Pha21* in the SA-induced immune pathway, we
171 transiently expressed two hairpin RNA (will generate 21 nt siRNA) of *Pha21*
172 (35S::hpPha21-1 and 35S::hpPha21-2) separately to knockdown *Pha21* by
173 agroinfiltration in *P. aphrodite* carrying hairpin RNA expression construct, phpPha21-
174 1 and phpPha21-2 (Fig 2A). Samples collected from the infiltrated site of orchid leaves
175 were used to detect the RNA level of *Pha21*, *PhaNPR1*, and *PhaPR1* by quantitative
176 RT-PCR (qRT-PCR). As shown in Fig 2A, the expression of *PhaNPR1* and *PhaPR1*
177 was decreased in both *Pha21*-silenced plants. In addition to transient knockdown of
178 *Pha21*, we also transiently overexpressed *Pha21* (35S::FLAG-Pha21) through
179 agroinfiltration in the leaves of *P. aphrodite.* However, transient overexpression of

180 *Pha21* in leaves did not significantly affect the RNA level of *PhaNPR1* and *PhaPR1*
181 (Fig 2B).

182 In addition, we also transiently silenced *PhaNPR1* (phpPhaNPR1) in *P. aphrodite*
183 to analyze the expression of *Pha21*. The results showed that the silenced *PhaNPR1*
184 showed decreased expression of *PhaPR1*; however, no obvious effect was observed on
185 the expression of *Pha21* (Fig 2C). These results suggest that *Pha21* is involved in the
186 expression of *PhaNPR1*, but not vice versa.

187 **Pha21 is induced by SA, jasmonic acid and ethylene**

188 We also tested whether *Pha21* was induced by defense-related plant hormones
189 including SA, jasmonic acid (JA) and ethylene (ET). Orchid plants were treated with
190 SA, JA and ET and samples were collected after treatment at different time points (up
191 to 72 h) for analysis of the expression of *Pha21* and the marker genes of each plant
192 hormone by qRT-PCR. The induction of *Pha21* by SA was observed at 1 h post-
193 treatment (Fig 2D). In addition, *Pha21* was also induced by JA and ET at 72 h and 12
194 h, respectively (Figs 2E and 2F). Our results showed that *Pha21* can respond to multiple
195 defense-related plant hormones, and SA induced *Pha21* expression at the very early
196 stage.

197 ***Pha21* plays a positive role in virus resistance**

198 To analyze whether *Pha21* plays a role in virus resistance, we first analyzed the
199 expression of *Pha21* in response to virus infection. We detected the RNA level of
200 *Pha21* in mock- or CymMV-inoculated *P. aphrodite* using qRT-PCR, and the results
201 showed that the RNA of *Pha21* is induced by CymMV infection (Fig 3A). Furthermore,
202 we transiently silenced or overexpressed *Pha21* in CymMV-infected *P. aphrodite* to

203 assay the effect on virus accumulation. Transient knockdown of *Pha21* had no
204 significant effect on CymMV accumulation (Fig 3B); whereas transient overexpression
205 of *Pha21* decreased CymMV accumulation (Fig 3C). In addition, we also generated
206 transgenic *P. equestris* overexpressing *Pha21* (35S::FLAG-Pha21). The expression of
207 *Pha21* is higher in the two individual asexually propagated progeny derived from two
208 T0 lines of transgenic *P. equestris* (Pha21#8 and Pha21#9) as compared to the non-
209 transgenic lines (WT) (Fig 3D). We further inoculated CymMV into individual
210 progenies derived from two transgenic lines, and the result showed that the
211 accumulation level of CymMV is decreased to 21% and 34% in the two transgenic lines
212 (Pha21#8 and Pha21#9) as compared to the non-transgenic lines (WT) (Fig 3D). Our
213 data suggest that Pha21 plays a positive role in virus resistance.

214 **Transgenic *Arabidopsis* overexpressing *Pha21* enhances antiviral resistance.**

215 To understand whether Pha21-mediated antiviral immunity is conserved in plants,
216 we generated the transgenic *Arabidopsis* (Col-0) overexpressing *Pha21* (35S::FLAG-
217 Pha21). Homozygous T3 plants derived from 3 T1 transgenic lines, At-Pha21#4, #5
218 and #6, were selected for further antiviral assay. The expression level of *Pha21* was
219 confirmed by qRT-PCR on the homozygote progenies (Fig 4A).

220 We mechanically inoculated *Cucumber mosaic virus* (CMV) to wild-type (WT)
221 and *Pha21* overexpressing *Arabidopsis* (At-Pha21#4, #5 and #6). Fourteen days post-
222 inoculation, the accumulation of CMV in WT and *Pha21* overexpressing *Arabidopsis*
223 were detected by qRT-PCR. The results showed that *Pha21* overexpressing
224 *Arabidopsis* decreased the accumulation of CMV (Fig 4A) compared to the WT, and

225 severe disease symptoms were observed on the WT but not in the *Pha21* overexpressing
226 *Arabidopsis* (Fig 4B).

227 **Subcellular localization of Pha21**

228 To better understand the role of Pha21 within cells, we first analyzed the
229 subcellular localization of Pha21. We fused green fluorescent protein (GFP) in the N-
230 or C-terminal of Pha21 driven by 35S promoter (pG-Pha21 and pPha21-G). The GFP-
231 fused Pha21 was further transfected into protoplasts isolated from *P. aphrodite.*
232 Twenty-four hours post-transfection, the localization of Pha21 was observed by using
233 a confocal microscope. The results indicated that the C-terminal GFP fusion protein
234 (Pha21-G) was observed in the nucleus in about 50% of cells; whereas the N-terminal
235 GFP fusion protein (Pha21-G) showed a similar result to our GFP control vector, which
236 had no nucleus-specific GFP (S2 Fig). Our data suggested that Pha21 can move into
237 the nucleus even without the predicated NLS signal.

238 **Pha21 and Pha13 does not confer transcriptional activation ability in yeast two-**
239 **hybrid assay**

240 Since both Pha21 and Pha13 have the ability to move into the nucleus (44), we tried
241 to understand whether Pha21 and Pha13 function as transcription factors. Therefore,
242 we analyzed its transcriptional activation ability through yeast two-hybrid (Y2H) assay.
243 We fused Pha21 and Pha13 to the Gal4 DNA binding domain to generate pGBKT7-
244 Pha21 and pGBKT7-Pha13. We transformed the pGBKT7-Pha21 or pGBKT7-Pha13
245 in the yeast strain AH109 without any Gal4 transcriptional activation domain (AD) and
246 further analyzed the transcriptional activation ability through the analysis of the
247 activation of reporter genes in yeast. As shown in S3 Fig, yeast with pGBKT7-Pha21

248 or pGBKT7-Pha13 cannot grow on the -Trp/Aureobasidin and -Trp/-Ade/-His medium,
249 and the colonies did not turn blue on X-α-Gal containing medium.

250 **Pha21 exhibits E3 ligase activity in which the A20 domain plays a major role**

251 Several A20 and/or AN1 domain containing proteins confer E3 ligase activity (44-
252 46, 53). To determine whether Pha21 functions as an E3 ligase, *in vitro* self-
253 ubiquitination E3 ligase activity assay was performed using FLAG-Ubiquitin (FLAG-
254 Ub), human E1 (hE1), human E2 (UBCH2, hE2), and purified His-tagged Pha21
255 (Pha21-His). The poly-ubiquitinated Pha21 can be detected in the presence of FLAG-
256 Ub, hE1, and hE2 using anti-FLAG antibody to detect FLAG-Ubiquitin. The results
257 revealed that Pha21 confers E3 ligase activity (Fig 5A).

258 Furthermore, we also analyzed the self-ubiquitination E3 ligase activity of the
259 A20 and/or AN1 domain of Pha21. We substituted the conserved cysteine and histidine
260 to glycine on the A20 and/or AN1 domains of Pha21-His (Fig 1) to generate A20
261 domain mutant (Pha21-A20m), AN1 domain mutant (Pha21-AN1m), and the double
262 mutant (Pha21-A20mAN1m) for E3 ligase activity analysis. As shown in Fig 5A, the
263 major E3 ligase activity was conferred by the A20 domain. A20 domain mutant and
264 double mutant of Pha21 showed lower self-ubiquitination E3 ligase activity than wild-
265 type Pha21 and Pha21-AN1 mutant (Fig 5A).

266 **A20 domain of Pha21 confers ubiquitin binding ability**

267 A20 and/or AN1 proteins have also been shown to confer ubiquitin binding ability
268 in animals and plants (44, 46, 47, 54, 55). To analyze whether Pha21 has ubiquitin
269 binding ability, Y2H assay was performed to verify the interaction using Pha21 as bait
270 and ubiquitin as prey. As shown in Fig 5B, Pha21 had a positive interaction with

271 ubiquitin, suggesting that Pha21 conferred ubiquitin binding ability. In addition, to
272 identify the ubiquitin binding domain of Pha21, a series of deletion mutants of Pha21
273 were generated, followed by Y2H assay. The result revealed that only truncated Pha21
274 fragments containing A20 domain ($Pha21^{1-136}$, $Pha21^{1-101}$, $Pha21^{1-40}$, $Pha21^{16-158}$,
275 $Pha21^{16-136}$, $Pha21^{16-101}$, $Pha21^{16-40}$) showed a positive interaction with ubiquitin,
276 suggesting that the A20 domain of Pha21 is responsible for the ubiquitin binding ability
277 (Fig 5B).

278 **Interaction analysis between orchid SAPs**

279 The A20/AN1 proteins may confer self-interaction and also interact with each other
280 (56). Therefore, we also analyzed whether Pha21 and Pha13 confer self-interaction and
281 also interact with each other. The Y2H assay was performed to verify the interaction
282 between Pha21 and Pha13. Our Y2H results suggested that Pha21 and Pha13 did not
283 interact with each other and no self-interaction of Pha21 or Pha13 was observed (S4
284 Fig).

285 ***Pha21* is involved in the expression of SA-induced PhaNPR1-dependent and -**
286 **independent genes.**

287 To further understand how Pha21 is involved in the antiviral immunity, we
288 performed transient silencing (35S::hpPha21-2) and overexpression assay
289 (35S::FLAG-Pha21) of *Pha21* in *P. aphrodite*, and analyzed the expression of the
290 previously identified PhaNPR1-dependent and -independent antiviral genes,
291 *Phalaenopsis* homolog of *RNA dependent RNA polymerase 1* (*PhaRdR1)* and
292 *Glutaredoxin C9 (PhaGRXC9)*, respectively (44). Our results indicated that transient
293 silencing of *Pha21* RNA increased the expression of *PhaRdR1*, while *PhaGRXC9*

294 remained unchanged (Fig 6A). Transient overexpression of *Pha21* RNA decreased the
295 expression of *PhaGRXC9*, but *PhaRdR1* remain unchanged (Fig 6B). Our data suggest
296 that *Pha21* affects the expression of *PhaRdR1* and *PhaGRXC9*.

297 ***Pha21* is involved in the expression of *PhaDCL4* and *PhaAGO1***

298 Because the RNAi pathway plays an important role in antiviral immunity (18, 19),
299 we analyzed whether *Pha21* is involved in the expression of core RNAi-related genes
300 including the *Phalaenopsis* homologs of *RdR2* (*PhaRdR2*, PATC124544), *RdR6*
301 (*PhaRdR6*, PATC131836), *DCL2* (*PhaDCL2*, PATC143544), *DCL4* (*PhaDCL4*,
302 PATC150652), *AGO1* (*PhaAGO1*, PATC157237), and *AGO10* (*PhaAGO10*,
303 PATC093469). Transient overexpression and silencing assay of *Pha21* was performed
304 in *P. aphrodite*. Overexpression of *Pha21* increased the RNA expression of *PhaDCL4*
305 and *PhaAGO1* (Fig 7A); whereas transient silencing of *Pha21* had no significant effect
306 on the RNA expression of RNAi-related genes (S5 Fig).

307 For comparison, we also analyzed the effect of Pha13 on the RNAi-related genes.
308 The results showed that transient overexpression of *Pha13* has no significant effect on
309 the expression of *PhaRdR2*, *PhaRdR6*, *PhaDCL2*, *PhaDCL4*, *PhaAGO1*, *and*
310 *PhaAGO10* (Fig 7B). Our results suggested that *Pha21* is involved in the expression of
311 *PhaDCL4* and *PhaAGO1*.

312 To see whether orchid *DCL4* (*PhaDCL4*) and *AGO1* (*PhaAGO1*) also play a role
313 in the antiviral immunity, we transiently silenced *PhaDCL4* and *PhaAGO1* through
314 delivering the hairpin RNA into *P. aphrodite* by agroinfiltration carrying hairpin RNA
315 expression constructs, phpPhaDCL4 and phpPhaAGO1. Our results showed that

316 transient silencing of *PhaDCL4* and *PhaAGO1* increased the accumulation of CymMV
317 (S6 Fig).

318 **The *Arabidopsis* homolog of *Pha21*, *AtSAP5*, is involved in the expression of**
319 ***DCL4* and *AGO1*.**

320 Our previous phylogenic analysis revealed that both Pha21 and Pha13 are closely
321 related to *Arabidopsis AtSAP5* (accession number: AT3G12630) (44). Therefore, we
322 also analyzed whether *AtSAP5* is involved in the expression of *DCL4* and *AGO1*. We
323 detected the expression of *DCL4* and *AGO1* in our previously generated transgenic
324 *Arabidopsis* overexpressing *AtSAP5* (AtSAP5-oe-4 and 11) and RNAi lines of *AtSAP5*
325 (AtSAP5-RNAi-3 and 7) by qRT-PCR (44). The expression level of *AtSAP5* was
326 confirmed by qRT-PCR (Fig 8A). Our results showed that slightly increased expression
327 of *DCL4* and *AGO1* were observed in overexpression transgenic lines, AtSAP5-oe-11
328 and decreased expression of *DCL4* and *AGO1* were observed in the RNAi lines,
329 AtSAP5-RNAi-3 and AtSAP5-RNAi-7 (Figs 8B and 8C). Our results suggest that
330 *AtSAP5* is important in the expression of *DCL4* and *AGO1*.

331 **A20 and AN1 domain of Pha21 play different roles in the expression of *PhaDCL4,***
332 ***PhaAGO1, PhaGRXC9* and virus resistance.**

333 Our previous results indicated that *Pha21* is involved in the expression of
334 *PhaDCL4*, *PhaAGO1*, and *PhaGRXC9* and virus accumulation (Figs 3C, 3D, 6B, and
335 7A). We further analyzed the roles of the A20 and/or AN1 domains of Pha21 in the
336 expression of *PhaDCL4*, *PhaAGO1*, *PhaGRXC9* and virus accumulation by
337 overexpression of Pha21 and Pha21 with mutation in the A20 and/or AN1 domain.
338 Therefore, we generated Pha21 with A20 domain mutant (Pha21A20m), AN1 domain

339 mutant (Pha21AN1m), and the double mutant (Pha21A20mAN1m) through the
340 substitution of the conserved cysteine and histidine to glycine on A20 and/or AN1
341 domain (Fig 1). We transiently overexpressed wild-type Pha21 or the mutants (A20
342 and/or AN1 domain mutant) in healthy or CymMV pre-infected *P. aphrodite*, and then
343 detected *PhaDCL4, PhaAGRO1, PhaGRXC9,* and CymMV. The results indicated that
344 overexpression of Pha21 A20 mutant (Pha21A20m) but not AN1 mutant (Pha21AN1m)
345 or A20/AN1 mutant (Pha21A20mAN1m) increased the expression of *PhaDCL4*, which
346 is similar to the wild-type Pha21 (Fig 9A). Overexpression of any Pha21 A20 and/or
347 AN1 mutant showed similar results to wild-type Pha21 with respect to increased
348 expression of *PhaAGO1* (Fig 9A). Although overexpression of wild-type and any
349 Pha21 A20 and/or AN1 mutant resulted in decreased expression of *PhaGRXC9* and
350 CymMV accumulation compared to the vector control, overexpression of wild-type
351 Pha21 showed a greater effect on the expression of *PhaGRXC9* and CymMV
352 accumulation compared to any Pha21 A20 and/or AN1 mutant (Fig 9). Our data suggest
353 that both the A20 and AN1 domains of Pha21 are required for expression of *PhaGRXC9*
354 and CymMV accumulation, and the AN1 domain plays a major role in the expression
355 of *PhaDCL4*. They also suggest that neither domain is required for the expression of
356 *PhaAGO1*.
357

358 ## Discussion

359 **Plant A20/AN1 proteins, Pha13, Pha21 and AtSAP5 share similar biochemical**
360 **properties and all involved in SA-mediated antiviral immunity**

361 In this report, we performed detailed analysis of a previously identified orchid
362 gene, *Pha21*, involved in SA and RNAi-mediated antiviral immunity. Pha21 shares
363 high protein sequence identity to our previously identified Pha13 (Fig. S7 in Chang et
364 al, 2018), and exhibits similar biochemical properties including self-E3 ligase, ubiquitin
365 binding abilities (Fig 5) and subcellular localization (S2 Fig). Similar to Pha13, our data
366 suggests that Pha21 is involved in the SA-signaling pathway downstream of SA and
367 upstream of the expression of *PhaNPR1* (Figs 2A, 2C and 2D). In addition, Pha13 and
368 Pha21 also positively mediate antiviral immunity in both transgenic orchid and
369 *Arabidopsis* overexpressing *Pha13* or *Pha21* (Figs 3D and 4) (44). Similar to *Pha13*,
370 our transgenic *Arabidopsis* overexpressing *Pha21* also enhanced resistance to virus
371 infection (Fig 4) (44). In addition, our previous report and the data presented here
372 indicate that similar to *Pha13* and *Pha21*, *Arabidopsis AtSAP5* is also induced by SA
373 at the early stage, is involved in expression of similar sets of SA mediated immune
374 responsive genes, and positively regulates antiviral immunity (44) (Fig 10).

375 **Pha13-mediated expression of *PhaGRXC9* and *PhaRdR1* are dominant during SA**
376 **treatment.**

377 Our previous study indicated that *Pha13* and *AtSAP5* plays a positive role in the
378 expression of genes involved in the RNAi pathway and SA-governed oxidoreductases,
379 *RdR1* and *GRXC9*, respectively. We demonstrated that both *PhaRdR1* and *PhaGRXC9*
380 play positive roles in antiviral immunity (44). In this study we found that *Pha21* has an
381 opposite role to *Pha13* in the expression of *PhaRdR1* and *PhaGRXC9* (Fig 6). As our
382 data indicates that the expression of *Pha13* is approximately 15 times higher than
383 *Pha21* in leaves of orchids as measured by digital PCR (S1B Fig), we suggest that the

384 effect of Pha21 on the expression of *PhaRdR1* and *PhaGRXC9* is minor, and Pha13-
385 mediated positive expression of *PhaGRXC9* and *PhaRdR1* are dominant during SA
386 treatment.

387 ***Pha21* and *AtSAP5* are all involved in expression of key genes in RNAi pathway,**
388 **but regulation of *PhaDCL4* and *PhaAGO1* by *Pha21* in orchid is different from**
389 **regulation of *DCL4* and *AGO1* by *AtSAP5* in *Arabidopsis***

390 Our data indicates that similar to *Arabidopsis DCL4* and *AGO1*, orchid *PhaDCL4*
391 and *PhaAGO1* also play a similar positive role in antiviral immunity in orchids as a
392 slight decrease in the RNA of *PhaDCL4* or *PhaAGO1* (approximately 40% decrease)
393 has a prominent effect on CymMV accumulation (approximately 100% increase) (S6
394 Fig), (19). Interestingly, our data suggests that Pha21 regulates antiviral immunity
395 partly through the effect on the RNAi pathway, as transient overexpression of *Pha21*
396 (1.6-folds) but not *Pha13* increased the expression of two *Phalaenopsis* orchid
397 homologs of RNAi-mediated antiviral immune genes, *DCL4* (*PhaDCL4*, 2-fold) and
398 *AGO1* (*PhaAGO1*, 1.6-fold) (Fig 7A). Once again, our data suggests that although
399 Pha13 and Pha21 both participate in SA regulated immunity, they act differently in
400 triggering downstream immune responsive genes.

401 Although the effect of *AtSAP5* on expression of *DCL4* and *AGO1* is not as
402 prominent as *Pha21*, our data shown here also indicates that *AtSAP5* is involved in the
403 expression of *DCL4* and *AGO*1. Our data indicates that only one overexpression line,
404 AtSAP5-oe-11 (expression increased about 7 times over AtSAP5) slightly increased
405 the expression of *DCL4* (40% increase) and *AGO1* (20% increase). However, both our
406 silencing lines, AtSAP5-RNAi-3 and -7 showed noticeable effect on the expression of

407 *DCL4* and *AGO1* (Fig 8). This suggests that *AtSAP5* is still important for the
408 maintenance of *DCL4* and *AGO1* expression.

409 **Pha13 and Pha21 showed no transcriptional activation activity by Y2H assay**

410 Although *Pha21* and *Pha13* are involved in expression of *PhaGRXC9*, *PhaRdR1*,
411 *PhaDCL4* and *PhaAGO1*, our Y2H analysis showed that Pha21 and Pha13 have no
412 transcriptional activation activity (S3 Fig). However, similar to other analyzed
413 A20/AN1 proteins, our biochemical assay indicated that both Pha21 and Pha13 confer
414 E3 ligase activity and ubiquitin binding ability, and A20 domain of Pha21 and Pha13
415 is the major domain exhibiting self-E3 ligase and ubiquitin binding activity (Fig 5) (44).
416 It has been well demonstrated that human A20 proteins (without an AN1 domain)
417 regulate the immune transcription factor NF-kB through ubiquitin editing activity
418 including E3 ligase and ubiquitin binding ability on different substrates (53). It is likely
419 that Pha21 and Pha13 may function in a similar manner to human A20 indirectly, rather
420 than directly function as transcription factors.

421 **A20 confers most E3 ligase and ubiquitin binding activity but the AN1 domain**
422 **also plays important roles in expression of immune responsive genes.**

423 Our previous domain functional analysis revealed that both the A20 and AN1
424 domains of Pha13 are required for regulation of *PhaRdR1*, *PhaGRXC9*, and virus
425 accumulation, and the AN1 domain of Pha13 is involved in the expression of *PhaNPR1*
426 (44). Here we also showed that A20 and AN1 domains of Pha21 are both required for
427 regulation of *PhaGRXC9* and CymMV accumulation, and the AN1 domain plays a
428 more important role in the expression of *PhaDCL4* (Fig 9). This indicates that although
429 A20 confers most E3 ligase and ubiquitin binding activity, the AN1 domain also plays

430 important roles in expression of immune responsive genes. Interestingly, our data
431 suggests that neither domain of Pha21 is required for the expression of *PhaAGO1*,
432 which suggests that protein regions other than A20 and AN1 domain in Pha21 are also
433 involved in the expression of *PhaAGO1* (Fig 9A).

434 **A20/AN1 proteins serve as important modulators in plant antiviral immunity**

435 Our previous data and the findings presented here indicate that A20/AN1 protein-
436 mediated antiviral immunity is conserved among plants, and A20/AN1 proteins may
437 work alone or in a cooperative manner in antiviral immunity to induce the expression
438 of the SA-mediated immune responsive genes, including *NPR1*, NPR1-independent
439 oxidoreductases genes (*GRXC9*), and genes involved in the RNAi pathway *(RdR1*,
440 *AGO1* and *Dicer 4*) (Fig 10).

441 ## Materials and Methods

442 **Plant materials and growth conditions**

443 Orchid variety, *Phalaenopsis aphrodite var. Formosa*, was purchased from
444 Taiwan Sugar Research Institute (Tainan, Taiwan). All orchid plants we used including
445 *P. aphrodite, P. equestris* and transgenic *P. equestris* (35S::FLAG-Pha21) were first
446 analyzed for the infection with two prevalent orchid viruses, *Odontoglossum ringspot*
447 *virus* (ORSV) and CymMV, as detected by RT-PCR with primer pairs, ORSV-
448 F/ORSV-R and CymMV-F/CymMV-R (S1 Table). Plants free from ORSV and
449 CymMV were maintained in greenhouse conditions with a controlled 12-h photoperiod
450 (200 μmol $m^{-2}s^{-2}$) at 25°C/25°C (day/night). The wild-type (WT) *Arabidopsis* WT (Col-
451 0) and all transgenic *Arabidopsis* were maintained in a greenhouse with a controlled

452 12-h photoperiod (200 μmol m-2s-2) at 22°C/22°C (day/night) for three to four weeks
453 before analysis. *Cucumber mosaic virus* (CMV) isolate 20 was maintained in the
454 *Arabidopsis* (Col-0) as inoculation source in our study.

455 **Sequence analysis**

456 The amino acid sequence of Pha21 was analyzed by the PROSITE database,
457 ExPASy Proteomics Server (http://ca.expasy.org/), and Conserved Domain Database
458 of NCBI database (http://www.ncbi.nlm.nih.gov/).

459

460 **Phytohormone treatment**

461 Sodium salicylate (50 mM) (Sigma, St. Louis, MO, USA), methyl jasmonate (45
462 μM) (Sigma), and aminocyclopropanecarboxylic acid (660 μM) (Sigma) were directly
463 rubbed on leaves of *P. aphrodite* by cotton swab. Leaf samples were collected at 0 h, 1
464 h, 3 h, 6 h, 12 h, 24 h, 48 h and 72 h after treatment.

465

466 **RNA isolation and real-time quantitative RT-PCR (qRT-PCR) detection**

467 Total RNA was extracted using the trizol method (Invitrogen, Carlsbad, CA, USA)
468 as described previously (51). The cDNA template for qPCR was synthesized from 500
469 ng of DNA-free RNA and oligo (dT) using PrimeScript RT Reagent Kit (Perfect Real
470 Time), following the manufacturer's instructions (Takara Bio, Shiga, Japan). qPCR was
471 performed using SYBR Green PCR Master Mix (Applied Biosystems, Foster, CA,
472 USA)) with ABI Prism 7500 sequence detection system (Applied Biosystems). Target
473 gene PCR products were sequenced to validate the correct analysis of gene targets.

474 *PhaUbiquitin 10* or *AtActin* was used as an internal quantification control.
475 Quantification of target gene expression was calculated according to the manufacturer's
476 instructions (Applied Biosystems). The primer pairs used in this study are listed in S1
477 Table.
478
479 **Droplet digital PCR**
480 Total RNA was extracted using the trizol method (Invitrogen, Carlsbad, CA, USA)
481 as described previously (51). For droplet digital PCR (ddPCR), DNA-free RNA (1 μg)
482 and oligodT primer were used for cDNA synthesis with PrimeScript RT Reagent Kit
483 (Perfect Real Time) following the manufacturer's instructions (Takara Bio). An amount
484 of 5 μl of 25X dilute cDNA was used as a template for ddPCR reaction (total 20 μl)
485 following the manufacturer's instructions (Bio-Rad, Hercules, CA, USA). The
486 sequence of FAM-labeled Taqman probes and primer pairs of Pha13 and Pha21 for
487 ddPCR are listed in S1 Table.
488
489 **Construction of transient silencing vector**
490 For construction of transient silencing vector of Pha21, the oligonucleotide pairs
491 Pha21-hpRNA-1-F/Pha21-hpRNA-1-R and Pha21-hpRNA-2-F/Pha21-hpRNA-2-R
492 (S1 Table) were used to amplify the hairpin dsDNA fragments. The hairpin dsDNA
493 fragments were cloned into the Gateway entry vector pENTR/D-TOPO (Thermo
494 Fisher-Scientific, Waltham, MA, USA) following the manufacturer's instructions to
495 generate pENTR-Pha21-hpRNA-1 and pENTR-Pha21-hpRNA-2. Then, LR Gateway
496 cloning reaction (Thermo Fisher-Scientific) was conducted to transfer the hairpin RNA

497 fragments from pENTR-Pha21-hpRNA into 35S promoter driven pB7GWIWG2(I) (57)
498 to obtain phpPha21-1 and phpPha21-2. The method for construction of the transient
499 silencing vector of *PhaNPR1, PhaDCL4, and PhaAGO1* (phpPhaNPR1, phpPhaDCL4,
500 and phpPhaAGO1) were similar to that described above, except the oligonucleotide
501 pairs PhaNPR1-hpRNA-F/PhaNPR1-hpRNA-R, PhaDCL4-hpRNA-F/PhaDCL4-
502 hpRNA-R, and PhaAGO1-hpRNA-F/ PhaAGO1-hpRNA-R (S1 Table) were used to
503 generate the hairpin dsDNA fragments.
504
505 **Construction of transient overexpression vector of Pha21, Pha21 A20 and/or AN1**
506 **domain mutant.**
507 To construct Pha21 transient overexpression vector, total *P. aphrodite* RNA was
508 used as a template to amplify the N-terminus FLAG-tagged Pha21 by RT-PCR with the
509 primer pairs FLAG-Pha21ORF-F/Pha21ORF-R (S1 Table). The amplified fragment
510 was cloned into Gateway entry vector pENTR/D-TOPO (Invitrogen) to generate
511 pENTR-FLAG-Pha21 following the manufacturer's protocol. Subsequently, LR
512 Gateway cloning reaction (Invitrogen) was performed to transfer the FLAG-Pha21
513 fragment from pENTR-FLAG-Pha21 into the 35S promoter driven pK2GW7 (57),
514 designated pPha21-oe. For generation of A20 and/or AN1 mutant on pPha21-oe (Fig.
515 1), site-directed mutagenesis was conducted by QuikChange Site-Directed Mutagenesis
516 Kit (Agilent Technologies, Santa Clara, CA, USA) and pPha21-oe was used as a
517 template. For A20 mutant, we substituted the conserved 3rd and 4th cysteine to glycine
518 at A20 (C35G and C38G). For AN1 mutant, we substituted the conserved 3rd cysteine
519 and 1st histidine to glycine at AN1 (C113G and H123G). The A20 mutated clones,

520 AN1 mutated clones, and the A20 and AN1 mutated clones, were designed as
521 pPha21A20m, pPha21AN1m, and pPha21A20mAN1m, respectively. Primer pairs used
522 for site directed mutagenesis are listed in S1 Table.

523 **Transgenic *Phalaenopsis* orchid**

524 For construction of overexpression vector to generate transgenic *Phalaenopsis*
525 orchid, the FLAG-Pha21 fragment was transferred from pENTR-FLAG-Pha21
526 (described above) into 35S promoter driven binary vector, pH2GW7 (57), to obtain
527 pHPha21. pHPha21 was used to generate transgenic *P. equestris* orchid using the
528 method described by Hsing et al. (58).

529

530 **Agroinfiltration**

531 Agroinfiltration was conducted as previously described by (51) with some
532 modification. Briefly, *A. tumefaciens* C58C1 (pTiB6S3ΔT)^{H} competent cells were
533 transformed with pCambia-CymMV, pB7GWIWG2, pK2GW7 and their derivatives
534 using an electroporation system (Bio-Rad Laboratories, Hercules, CA, USA). Then, the
535 *A. tumefaciens* strains were incubated at 28°C until the optical density, OD_{600}, reached
536 0.8–1.0. After centrifugation, cells were resuspended in 20 ml AB-MES medium (17.2
537 mM K_2HPO_4, 8.3 mM NaH_2PO_4, 18.7 mM NH_4Cl, 2 mM KCl, 1.25 mM $MgSO_4$, 100
538 μM $CaCl_2$, 10 μM $FeSO_4$, 50 mM MES, 2% glucose (w/v), pH 5.5) with 200 μm
539 acetosyringone (59), and cultured overnight. The overnight culture was centrifuged
540 (3000 rpm, 10 min, in room temperature), supernatant was removed and the *A.*
541 *tumefaciens* culture was resuspended in 2 ml of infiltration medium containing 50%
542 MS medium (1/2 MS salt supplemented with 0.5% sucrose (w/v), pH 5.5), 50% AB-

543 MES and 200 μm acetosyringone (59). The infiltration medium containing the
544 transformed *A. tumefaciens* was applied for infiltration.
545
546 ***Cymbidium mosaic virus* (CymMV) and *Cucumber mosaic virus* (CMV) inoculation**
547 **and accumulation assay**
548 To assay the effect of Pha21, PhaDCL4, or PhaAGO1 in CymMV accumulation,
549 we first inoculated CymMV in *P. aphrodite* through the infiltration of *A. tumefaciens*
550 carrying pCambia-CymMV (described above) in the leaf tip of *P. aphrodite*. The
551 CymMV-infected *P. aphrodite* was maintained at least 14 days before further analysis.
552 To assay the effect of transient silencing (Pha21, PhaDCL4, or PhaAGO1) or transient
553 overexpression (Pha21, or the derived mutants), *A. tumefaciens* carrying the control
554 vector pB7GWIWG2 (for silencing), pK2GW7 (for overexpression), silencing vectors
555 or overexpression vectors (described above) were infiltrated into the leaves. After
556 agroinfiltration, a pair of disks (6 mm diameter) were immediately (defined as 0 dpi)
557 collected from both the control and assay vector infiltrated regions. After 5 dpi, another
558 pair of disks were collected from the same infiltrated region. Total RNA extracted from
559 the samples was used as a template to analyze the accumulation of CymMV by use of
560 qRT-PCR. The fold change of CymMV accumulation at 0 dpi to 5 dpi was calculated
561 for relative quantification.
562 For inoculation with CMV, CMV-infected *Arabidopsis* leaves were ground with
563 0.01 M potassium phosphate buffer by pestle and mortar for use as the inoculation
564 source. Four-week-old *Arabidopsis* leaves were inoculated mechanically (pre-dusted
565 with 300-mesh Carborundum) with the CMV inoculation source. After 14 dpi, the

566 disease symptoms were observed, and three disks from three different distal leaves were
567 collected for CMV accumulation analysis by use of qRT-PCR. Primers used for CMV
568 detection are listed in S1 Table.
569
570 **Preparation and transfection of protoplasts**
571 For construction of vectors used for subcellular localization analysis, the primer
572 pairs, Pha21-ORF-F/Pha21-ORF-R and Pha21-ORF-F/Pha21-ORF-non-stop-R (S1
573 Table) were used to amplify 2 sets of Pha21 ORF (with or without a stop codon). The
574 amplified fragment was cloned into Gateway entry vector pENTR/D-TOPO (Invitrogen)
575 to generate pENTR-Pha21 and pENTR-Pha21-non-stop following the manufacturer's
576 protocol. Subsequently, LR Gateway cloning reaction (Invitrogen) was performed to
577 transfer ORF fragment of *Pha21* from pENTR-Pha21 into p2FGW7 driven by 35S
578 promoter (57) to obtain N-terminal GFP fused clones (pG-Pha21). To obtain C-terminal
579 GFP-fused clones (pPha21-G), we transferred and pENTR-Pha21-non-stop into
580 p2GWF7.
581 Protoplast isolation and transfection were as described by Lu et al. (51).
582 Transformed protoplasts were detected for florescence signals by confocal microscopy
583 (Zeiss LSM 780, plus ELYRA S.1) with excitation at 488 nm and emission at 500 to
584 587 nm for GFP, and excitation at 543 nm and emission at 600 to 630 nm for mCherry.
585
586 **Transcriptional activation ability assay**
587 The Pha13 and Pha21 ORF was amplified by PCR with gene specific primer pairs,
588 NdeI-Pha13-F/EcoR1-Pha13-R and NdeI-Pha21-F/BamH1-Pha21-R, respectively (S1

589 Table). The amplified ORF fragment was then cloned into the pGBKT7 vector (Takara
590 Bio) to generate the pGBKT7-Pha13 and pGBKT7-Pha21 constructs, which fused to
591 Gal4 BD sequence. These constructs were individually transformed into AH109 yeast
592 strain (Takara Bio) and the self-activation ability was analyzed. The transformation and
593 selection procedure was performed following the Yeast Protocols HandBook (Takara
594 Bio). Transformants were selected on SD/-Trp (tryptophan) medium. The expression
595 of reporter genes in yeast were tested on different selection media; SD/-
596 Trp/Aureobasidin was used to test for activation of the AUR1-C (inositol phosphoryl
597 ceramide synthase) reporter against Aureobasidin A, SD/-Trp/X-α-Gal medium was
598 used to test for activation of α-galactosidase, and SD/-Trp/-Ade/-His medium was used
599 to test for induction of the ADE2 and HIS3 reporters. The yeast containing Gal4 DNA-
600 BD fused with murine p53 (pGBKT7-53) and the Gal4 AD fused with SV40 large T-
601 antigen (pGADT7-T) from the Matchmaker Gold Yeast Two-Hybrid System kit
602 (Takara Bio) were used as positive control. The yeast containing Gal4 DNA-BD fused
603 with lamin (pGBKT7-Lam) and the pGADT7-T from the Matchmaker Gold Yeast
604 Two-Hybrid System kit (Takara Bio) were used as a negative control.
605
606 **Construction, expression, and purification of recombinant proteins**
607 Full-length Pha21, or Pha21 A20 and/or AN1 domain mutant fragments were
608 amplified by PCR with primer pairs NdeI-Pha21-F/NotI-Pha21-R (S1 Table) using
609 pPha21-oe, pPha21A20m, pPha21AN1m, and pPha21A20mAN1m as templates. The
610 amplified fragments were cloned into the pET24b expression vector (Merck, Darmstadt,
611 Germany) to produce fused C-terminal histidine tag (His-tag) expression plasmids,

612 pETPha21, pETPha21A20m, pETPha21AN1m and pETPha21A20mAN1m. The
613 constructed plasmids were transformed into *Escherichia coli* strain BL21 (DE3) for
614 protein expression. Bacteria were cultured at 37°C to an OD600 of 0.5, then transferred
615 to 25°C, for 1.5 h. Then, isopropylthio-β-galactoside (IPTG; Sigma) was added to a
616 final concentration of 1 mM for protein induction. His-tagged recombinant protein was
617 purified by TALON Superflow (GE Healthcare Life Sciences, Pittsburgh, PA, USA)
618 according to the manufacturer's description. His-tagged recombinant protein was
619 eluded with 250 mM imidazole (Sigma).

620 **E3 ubiquitin ligase activity assay**

621 *In vitro* ubiquitination assays were performed as described by (45) with
622 modification. An amount of 3 μg purified His-tagged recombinant proteins (*Pha21* or
623 derived mutants) was used for each ubiquitination reaction. Reactions were incubated
624 at 30°C for 3 hours and analyzed by SDS-PAGE followed by immunoblot analysis.
625 Blots were probed using anti-FLAG antibodies (Sigma) followed by HRP conjugated
626 goat anti-mouse antibodies (GE Healthcare Life Sciences).

627

628 **Yeast two-hybrid assay**

629 For the ubiquitin binding ability assay, the pGBKT7-Pha21 (described above)
630 was used as a bait vector. To map the region of Pha21 for ubiquitin binding, a deletion
631 mutant of Pha21 was generated by PCR amplification with the primer pairs described
632 in S1 Table. The PCR-amplified fragment was individually cloned to pGBKT7 and
633 used as a bait vector (Fig 5B). Full length of orchid ubiquitin was amplified by RT-
634 PCR with the primer pair, NdeI-PhaUBQ-F/BamHI-PhaUBQ-R, and cloned into

635 pGADT7 vector (Takara Bio) to generate pGADT7-UBQ as a prey vector. pGBKT7-
636 Pha21 and pGADT7-UBQ was co-transformed into AH109 yeast strain for yeast two-
637 hybrid assay by using the Make Your Own "Mate & Plate" Library System (Takara
638 Bio) following the user manual. Yeast strains containing the appropriate bait and prey
639 plasmids were cultured in liquid 2-dropout medium (leucine$^-$ and tryptophan$^-$)
640 overnight. The overnight yeast culture was diluted to an OD600 of 0.06 and spotted on
641 selection plates (containing histidine$^-$, leucine$^-$, tryptophan$^-$ for growth assay.

642 For the interaction analysis between Pha21 and Pha13, full-length Pha13
643 fragment was amplified by PCR with primer pair NdeI-Pha13-F/EcoR1-Pha13-R (S1
644 Table). The Pha13 fragments were cloned into pGBKT7 and pGADT7 vector to
645 generate pGBKT7-Pha13 as the bait vector and pGADT7-Pha13 as the prey vector. The
646 full-length of Pha21 previously used to generate the pGBKT7-Pha21 (described above)
647 was also cloned into pGADT7 to generate pGADT7-Pha21 as prey vector. The
648 pGBKT7-Pha21, pGBKT7-Pha13, pGADT7-Pha21, and pGADT7-Pha13 were co-
649 transformed into AH109 yeast strain for yeast two-hybrid assay as described above.
650 The pGBKT7-53 and pGADT7-T from the Matchmaker Gold Yeast Two-Hybrid
651 System kit were used as a positive control.

652

653 **Accession numbers**

654 Pha21 (PATC144963)，Pha13 (PATC148746)，PhaPR1 (PATC126136)，PhaNPR1
655 (PATC135791)，PhadR1 (PATC143146)，PhaRdR2 (PATC124544)，PhaRdR6
656 (PATC131836)，PhaDCL2 (PATC143544)，PhaDCL4 (PATC150652)，PhaAGO1
657 (PATC157237)，PhaAGO10 (PATC093469)，PhaGRXC9 (PATC068819)，

PhaUBQ10 (PATC230548)，PhaJAZ1 (PATC141437)，PhaACO2 (PATC139319)，AtActin (At3G18780)，AtSAP5 (AT3G12630)，DCL4 (AT5G20320)，AGO1 (AT1G48410)，OsSAP3 (LOC_Os01g56040.1)，OsSAP5 (LOC_Os02g32840.1)

Acknowledgments

We thank Shu-Chen Shen from the Confocal Microscope Core Facility at Academia Sinica for assistance in confocal microscopy images and Chii-Gong Tong from the Gene Transgenic Room at Academia Sinica for orchid transformation.

670 **References**

671 1. Pieterse CM, Leon-Reyes A, Van der Ent S, Van Wees SC. Networking by small-
672 molecule hormones in plant immunity. Nat Chem Biol. 2009;5(5):308-16.
673 2. White R. Acetylsalicylic acid (aspirin) induces resistance to tobacco mosaic virus
674 in tobacco. Virology. 1979;99(2):410-2.
675 3. Chivasa S, Murphy AM, Naylor M, Carr JP. Salicylic acid interferes with tobacco
676 mosaic virus replication via a novel salicylhydroxamic acid-sensitive mechanism. The
677 Plant Cell. 1997;9(4):547-57.
678 4. Fu ZQ, Dong X. Systemic acquired resistance: turning local infection into global
679 defense. Annual review of plant biology. 2013;64:839-63.
680 5. Ausubel FM. Are innate immune signaling pathways in plants and animals
681 conserved? Nature Immunology. 2005;6:973-9.
682 6. Boller T, Felix G. A renaissance of elicitors: perception of microbe-associated
683 molecular patterns and danger signals by pattern-recognition receptors. Annual
684 review of plant biology. 2009;60:379-406.
685 7. Jones JD, Dangl JL. The plant immune system. Nature. 2006;444(7117):323-9.
686 8. Yang H, Gou X, He K, Xi D, Du J, Lin H, et al. BAK1 and BKK1 in Arabidopsis thaliana
687 confer reduced susceptibility to turnip crinkle virus. European journal of plant
688 pathology. 2010;127(1):149-56.
689 9. Kørner CJ, Klauser D, Niehl A, Domínguez-Ferreras A, Chinchilla D, Boller T, et al.
690 The immunity regulator BAK1 contributes to resistance against diverse RNA viruses.
691 Molecular plant-microbe interactions. 2013;26(11):1271-80.
692 10. Niehl A, Wyrsch I, Boller T, Heinlein M. Double-stranded RNAs induce a pattern-
693 triggered immune signaling pathway in plants. New Phytologist. 2016;211(3):1008-19.
694 11. Holmes FOJBG. Local lesions in tobacco mosaic. 1929;87(1):39-55.
695 12. HoLMEs FOJP. Inheritance of resistance to tobacco-mosaic disease in the pepper
696 (Capsicum sp.). 1937;27:637-42.
697 13. Holmes FOJP. Inheritance of resistance to tobacco-mosaic disease in tobacco.
698 1938;28(8).
699 14. Holmes FO. Inheritance of resistance to viral diseases in plants. Advances in
700 virus research. 2: Elsevier; 1954. p. 1-30.
701 15. Tsuda K, Katagiri FJCoipb. Comparing signaling mechanisms engaged in pattern-
702 triggered and effector-triggered immunity. 2010;13(4):459-65.
703 16. Ross AFJV. Localized acquired resistance to plant virus infection in hypersensitive

704 hosts. 1961;14(3):329-39.
705 17. Ross AFJV. Systemic acquired resistance induced by localized virus infections in
706 plants. 1961;14(3):340-58.
707 18. Ding S-W, Voinnet O. Antiviral immunity directed by small RNAs. Cell.
708 2007;130(3):413-26.
709 19. Zhang C, Wu Z, Li Y, Wu J. Biogenesis, function, and applications of virus-derived
710 small RNAs in plants. Frontiers in microbiology. 2015;6:1237.
711 20. Sharma N, Sahu PP, Puranik S, Prasad MJMb. Recent advances in plant–virus
712 interaction with emphasis on small interfering RNAs (siRNAs). 2013;55(1):63-77.
713 21. Blevins T, Rajeswaran R, Shivaprasad PV, Beknazariants D, Si-Ammour A, Park H-S,
714 et al. Four plant Dicers mediate viral small RNA biogenesis and DNA virus induced
715 silencing. 2006;34(21):6233-46.
716 22. Deleris A, Gallego-Bartolome J, Bao J, Kasschau KD, Carrington JC, Voinnet OJS.
717 Hierarchical action and inhibition of plant Dicer-like proteins in antiviral defense.
718 2006;313(5783):68-71.
719 23. Vaucheret HJTips. Plant argonautes. 2008;13(7):350-8.
720 24. Carbonell A, Carrington JCJCoipb. Antiviral roles of plant ARGONAUTES.
721 2015;27:111-7.
722 25. Yu D, Fan B, MacFarlane SA, Chen Z. Analysis of the involvement of an inducible
723 Arabidopsis RNA-dependent RNA polymerase in antiviral defense. Molecular Plant-
724 Microbe Interactions. 2003;16(3):206-16.
725 26. Yang S-J, Carter SA, Cole AB, Cheng N-H, Nelson RS. A natural variant of a host
726 RNA-dependent RNA polymerase is associated with increased susceptibility to viruses
727 by Nicotiana benthamiana. Proceedings of the National Academy of Sciences of the
728 United States of America. 2004;101(16):6297-302.
729 27. Liu Y, Gao Q, Wu B, Ai T, Guo X. NgRDR1, an RNA-dependent RNA polymerase
730 isolated from Nicotiana glutinosa, was involved in biotic and abiotic stresses. Plant
731 Physiology and Biochemistry. 2009;47(5):359-68.
732 28. Li Y, Muhammad T, Wang Y, Zhang D, Crabbe MJC, Liang YJPJOB. Salicylic acid
733 collaborates with gene silencing to tomato defense against tomato yellow leaf curl
734 virus (TYLCV). 2018.
735 29. Campos L, Granell P, Tárraga S, López-Gresa P, Conejero V, Bellés JM, et al. Salicylic
736 acid and gentisic acid induce RNA silencing-related genes and plant resistance to RNA
737 pathogens. 2014;77:35-43.

738 30. Alamillo JM, Saénz P, García JAJTPJ. Salicylic acid-mediated and RNA-silencing
739 defense mechanisms cooperate in the restriction of systemic spread of plum pox virus
740 in tobacco. 2006;48(2):217-27.
741 31. Xie Z, Fan B, Chen C, Chen Z. An important role of an inducible RNA-dependent
742 RNA polymerase in plant antiviral defense. Proceedings of the National Academy of
743 Sciences. 2001;98(11):6516-21.
744 32. Hunter LJR, Westwood JH, Heath G, Macaulay K, Smith AG, MacFarlane SA, et al.
745 Regulation of RNA-dependent RNA polymerase 1 and isochorismate synthase gene
746 expression in Arabidopsis. PLoS ONE. 2013;8(6):e66530.
747 33. Zhou M, Wang W, Karapetyan S, Mwimba M, Marqués J, Buchler NE, et al. Redox
748 rhythm reinforces the circadian clock to gate immune response. 2015;523(7561):472.
749 34. Mou Z, Fan W, Dong X. Inducers of plant systemic acquired resistance regulate
750 NPR1 function through redox changes. Cell. 2003;113(7):935-44.
751 35. Tada Y, Spoel SH, Pajerowska-Mukhtar K, Mou Z, Song J, Wang C, et al. Plant
752 immunity requires conformational charges of NPR1 via S-nitrosylation and
753 thioredoxins. Science. 2008;321(5891):952-6.
754 36. Herrera-Vásquez A, Salinas P, Holuigue LJFips. Salicylic acid and reactive oxygen
755 species interplay in the transcriptional control of defense genes expression.
756 2015;6:171.
757 37. Cao H, Bowling SA, Gordon AS, Dong X. Characterization of an Arabidopsis mutant
758 that is nonresponsive to inducers of systemic acquired resistance. The Plant Cell.
759 1994;6(11):1583-92.
760 38. Delaney T, Friedrich L, Ryals J. Arabidopsis signal transduction mutant defective
761 in chemically and biologically induced disease resistance. Proceedings of the National
762 Academy of Sciences. 1995;92(14):6602-6.
763 39. Shah J, Tsui F, Klessig DF. Characterization of a s alicylic a cid-i nsensitive mutant
764 (sai1) of Arabidopsis thaliana, identified in a selective screen utilizing the SA-inducible
765 expression of the tms2 gene. Molecular Plant-Microbe Interactions. 1997;10(1):69-78.
766 40. Wong CE, Carson RA, Carr JP. Chemically induced virus resistance in Arabidopsis
767 thaliana is independent of pathogenesis-related protein expression and the NPR1 gene.
768 Molecular plant-microbe interactions. 2002;15(1):75-81.
769 41. Kachroo P, Yoshioka K, Shah J, Dooner HK, Klessig DF. Resistance to turnip crinkle
770 virus in Arabidopsis is regulated by two host genes and is salicylic acid dependent but
771 NPR1, ethylene, and jasmonate independent. The Plant Cell. 2000;12(5):677-90.

772 42. Vij S, Tyagi AK. A20/AN1 zinc-finger domain-containing proteins in plants and
773 animals represent common elements in stress response. Functional & integrative
774 genomics. 2008;8(3):301-7.
775 43. Giri J, Dansana PK, Kothari KS, Sharma G, Vij S, Tyagi AK. SAPs as novel regulators
776 of abiotic stress response in plants. Bioessays. 2013;35(7):639-48.
777 44. Chang L, Chang H-H, Chang J-C, Lu H-C, Wang T-T, Hsu D-W, et al. Plant A20/AN1
778 protein serves as the important hub to mediate antiviral immunity.
779 2018;14(9):e1007288.
780 45. Kang M, Fokar M, Abdelmageed H, Allen RD. Arabidopsis SAP5 functions as a
781 positive regulator of stress responses and exhibits E3 ubiquitin ligase activity. Plant
782 molecular biology. 2011;75(4-5):451-66.
783 46. Kang M, Lee S, Abdelmageed H, Reichert A, Lee HK, Fokar M, et al. Arabidopsis
784 stress associated protein 9 mediates biotic and abiotic stress responsive ABA signaling
785 via the proteasome pathway. Plant, cell & environment. 2017;40(5):702-16.
786 47. Choi H, Han S, Shin D, Lee S. Polyubiquitin recognition by AtSAP5, an A20-type
787 zinc finger containing protein from Arabidopsis thaliana. Biochemical and biophysical
788 research communications. 2012;419(2):436-40.
789 48. Verhelst K, Carpentier I, Kreike M, Meloni L, Verstrepen L, Kensche T, et al. A20
790 inhibits LUBAC-mediated NF-κB activation by binding linear polyubiquitin chains via its
791 zinc finger 7. The EMBO Journal. 2012;31:3845-55.
792 49. Wertz IE, O'rourke KM, Zhou H, Eby M. De-ubiquitination and ubiquitin ligase
793 domains of A20 downregulate NF-kappaB signalling. Nature. 2004;430(7000):694.
794 50. Mattera R, Tsai YC, Weissman AM, Bonifacino JS. The Rab5 guanine nucleotide
795 exchange factor Rabex-5 binds ubiquitin (Ub) and functions as a Ub ligase through an
796 atypical Ub interacting motif and a zinc finger domain. The Journal of Biological
797 Chemistry. 2006;281:6874-83.
798 51. Lu HC, Hsieh MH, Chen CE, Chen HH, Wang HI, Yeh HH. A high-throughput virus-
799 induced gene-silencing vector for screening transcription factors in virus-induced plant
800 defense response in orchid. Molecular Plant-Microbe Interactions. 2012;25(6):738-46.
801 52. Chang C-H, Wang H-I, Lu H-C, Chen C-E, Chen H-H, Yeh H-H, et al. An efficient RNA
802 interference screening strategy for gene functional analysis. BMC genomics.
803 2012;13(1):491.
804 53. Ma A, Malynn BA. A20: linking a complex regulator of ubiquitylation to immunity
805 and human disease. Nature reviews Immunology. 2012;12(11):774.

806 54. Hishiya A, Iemura Si, Natsume T, Takayama S, Ikeda K, Watanabe K. A novel
807 ubiquitin-binding protein ZNF216 functioning in muscle atrophy. The EMBO Journal.
808 2006;25(3):554-64.
809 55. Miyata N, Okumoto K, Mukai S, Noguchi M, Fujiki Y. AWP1/ZFAND6 Functions in
810 Pex5 Export by Interacting with Cys-Monoubiquitinated Pex5 and Pex6 AAA ATPase.
811 Traffic. 2012;13(1):168-83.
812 56. Giri J, Vij S, Dansana PK, Tyagi AK. Rice A20/AN1 zinc-finger containing stress-
813 associated proteins (SAP1/11) and a receptor-like cytoplasmic kinase (OsRLCK253)
814 interact via A20 zinc-finger and confer abiotic stress tolerance in transgenic
815 Arabidopsis plants. New Phytologist. 2011;191(3):721-32.
816 57. Karimi M, Inzé D, Depicker A. GATEWAY™ vectors for Agrobacterium-mediated
817 plant transformation. Trends in plant science. 2002;7(5):193-5.
818 58. Hsing H-X, Lin Y-J, Tong C-G, Li M-J, Chen Y-J, Ko S-S. Efficient and heritable
819 transformation of Phalaenopsis orchids. Botanical studies. 2016;57(1):30.
820 59. Wu H-Y, Liu K-H, Wang Y-C, Wu J-F, Chiu W-L, Chen C-Y, et al. AGROBEST: an
821 efficient Agrobacterium-mediated transient expression method for versatile gene
822 function analyses in Arabidopsis seedlings. Plant methods. 2014;10(1):19.

823

824 ## Supporting information

825 **S1 Table. Primers and probes used in this study**

826 **S1 Fig. Expression analysis of *Pha21* and *Pha13* in *P. aphrodite*.** (A) Expression
827 level of *Pha21* was analyzed by qRT-PCR from the root, leaf, petal, sepal, column, and
828 lip of *P. aphrodite*. The RNA level of the root was set to 1. Data represent mean ± SD;
829 n = 3 technical replicates; different letters indicate statistically significant differences
830 analyzed by one-way analysis of variance (ANOVA) Tukey's test ($P < 0.05$). The
831 experiment was repeated at least three times with similar results, and one representative
832 experiment is shown. *PhaUbiquitin 10* was used as an internal control for normalization.
833 (B) Absolute quantitative analysis of *Pha13* and *Pha21* expression. The mRNA copy
834 numbers of *Pha13* and *Pha21* in leaves of *P. aphrodite* were absolutely quantified by

835 droplet digital PCR. Total RNA (ng) was used for normalization. Data represent mean
836 ± SD; n = 3 biological replicates; **, $P < 0.01$, Student's t test compared Pha13 with
837 Pha21
838
839 **S2 Fig. Subcellular localization of Pha21.** Green fluorescent protein (GFP) or N- and
840 C- terminal GFP-fused Pha21 (G-Pha21 and Pha21-G) were co-transfected with
841 nucleus localization signal fused red fluorescence protein (NLS-RFP) into protoplasts
842 of *P. aphrodite*. Fluorescence was detected by confocal microscopy after transfection.
843 Scale bars represent 10 μm.
844
845 **S3 Fig. Transcriptional activation analysis of Pha13 and Pha21.** Yeast two-hybrid
846 assay was used to analyze the transcriptional activation. AH109 is the yeast strain used
847 in this assay. The pGBKT7-Pha13 and pGBKT7-Pha21 indicates that yeast encodes
848 Pha13 or Pha21 fused to the Gal4 DNA binding domain. The pGBKT7-53, pGADT7-
849 T, and pGBKT7-Lam provided in Matchmaker Gold Yeast Two-Hybrid System kit
850 were used as a positive (pGBKT7-53 + pGADT7-T) and negative (pGBKT7-Lam +
851 pGADT7-T) control. The -Trp indicates the medium without tryptophan. The -
852 Trp/Aureobasidin was used to test for activation of the inositol phosphoryl ceramide
853 synthase (AUR1-C) for Aureobasidin A resistance. The -Trp/X-α-Gal medium was
854 used to test for activation of α-galactosidase, and -Trp/-Ade/-His indicate the selective
855 medium without tryptophan, adenine, and histidine
856

857 **S4 Fig. Interaction analysis of Pha21 and Pha13.** Yeast two-hybrid assay was
858 performed to analyze the interaction between Pha21 and Pha13. The pGBKT7 and
859 pGADT7 were used as a negative control. The pGBKT7-53 and pGADT7-T (provided
860 in the Matchmaker Gold Yeast Two-Hybrid System kit), and pGBKT7-Pha21 and
861 pGADT7-PhaUBQ were used as a positive control. The 2DO indicates the dropout
862 selective medium without Leucine and Tryptophan. The 3DO indicates dropout
863 selective medium without the Leucine, Tryptophan, and Histidine.
864
865 **S5 Fig. Transient silencing of *Pha21* has no significant effect on the expression of**
866 **RNAi-related genes.** The expression levels of *Pha21*, *PhaRdR2*, *PhaRdR6*, *PhaDCL2*,
867 *PhaDCL4*, *PhaAGO1*, and *PhaAGO10* were analyzed by qRT-PCR from leaves of *P.*
868 *aphrodite* infiltrated with agrobacterium carrying control vector (Vector) or knock
869 down *Pha21* (hpPha21-2). The RNA level of plants infiltrated with control vector was
870 set to 1. Data represent mean ± SD; n = 3 biological replicates; **, $P < 0.01$, Student's
871 t-test compared to Vector. *PhaUbiquitin* 10 was used as an internal control for
872 normalization.
873
874 **S6 Fig. *PhaDCL4* and *PhaAGO1* are involved in antiviral immunity.** The expression
875 level of *PhaDCL4*, *PhaAGO1*, and CymMV accumulation level were analyzed by qRT-
876 PCR from leaves of CymMV-infected *P. aphrodite* infiltrated with agrobacterium
877 carrying vector (Vector); hairpin RNA (hpRNA) vector to knock down *PhaDCL4*
878 (hpPhaDCL4, A), or *PhaAGO1* (hpPhaAGO1, B). The RNA level of plants infiltrated
879 with control vector was set to 1. Data represent mean ± SD; n = 3 biological replicates;

880 **, $P < 0.01$; *, $P < 0.05$, Student's t test compared to Vector. (A-B) *PhaUbiquitin 10*
881 was used as an internal control for normalization.

882 ## Figure Captions

883 **Fig 1. Sequence analysis of Pha21** (A) A schematic representation of domain
884 organization of Pha21. The open rectangle indicates the entire protein. A20 (dark grey
885 rectangle) and AN1 (light grey rectangle) and 21-nucleotide position (short black line)
886 used for designing hairpin RNA of Pha21 (hpPha21-1 and hpPha21-2) are indicated.
887 (B) Amino sequence alignment of A20/AN1 zinc finger domains of Pha21 with stress-
888 associated proteins from *Phalaenopsis aphrodite* (*Pha13,* accession number:
889 PATC148746), *Arabidopsis thaliana* (*AtSAP5*, accession number: AT3G12630), and
890 *Oryza sativa* (*OsSAP3*, accession number: LOC_Os01g56040.1; *OsSAP5*, accession
891 number: LOC_Os02g32840.1) is shown. The black box indicates the conserved amino
892 acid sequences. The black triangle indicates the conserved cysteine (C) and histidine
893 (H) residues. (C) Primary sequence organization of A20 and AN1 domains. Xn: the
894 number of amino acid residues between zinc ligands. (B-C) The mutation positions for
895 domain functional analysis are indicated with a blue triangle.

896

897 **Fig 2. *Pha21* is involved in the expression of *PhaPR1* and *PhaNPR1,* and responds**
898 **to phytohormone treatment.** (A and B) qRT-PCR was performed to quantify the RNA
899 level of *Pha21, PhaNPR1*, and *PhaPR1* from leaves of *P. aphrodite* infiltrated with
900 agrobacterium carrying control vector (Vector); hairpin RNA vector to knock down
901 *Pha21* (hpPha21-1 and hpPha21-2; A); and overexpression vector of *Pha21* (Pha21-oe;
902 B). The RNA level of plants infiltrated with control vector was set to 1. (C) Transient

903 silencing of *PhaNPR1*. qRT-PCR was performed to quantify the RNA level of
904 *PhaNPR1, PhaPR1* and *Pha21* from leaves of *P. aphrodite* infiltrated with
905 agrobacterium carrying control vector (Vector) or hairpin RNA (hpRNA) vector to
906 knock down *PhaNPR1* (hpPhaNPR1). The RNA level of plants infiltrated with control
907 vector was set to 1. (A to C) Data represent mean ± SD; n = 3 biological replicates; **,
908 $P < 0.01$; *, $P < 0.05$, Student's t test compared to Vector. (D to F) Time-course
909 expression of *Pha21* under different plant hormone treatments in *P. aphrodite*. qRT-
910 PCR was performed to analyze the RNA level of *Pha21* from leaves treated with SA
911 (D), JA (E), and ET (F) at different hours (h) post-treatment. Buffer treatment was used
912 as a mock control. Results of qRT-PCR were relative to that of mock at individual time
913 courses for relative quantification. The RNA level at 0 h was set to 1 for comparison
914 between different time courses. *PhaPR1* and *PhaNPR1* were SA-responsive marker
915 genes. *PhaJAZ1* and *PhaACO2* were JA and ET–responsive marker genes, respectively.
916 Data represent mean ± SD; n = 3 biological replicates; **, $P < 0.01$; *, $P < 0.05$,
917 Student's t test compared to 0 h. (A-F) *PhaUbiquitin 10* was used as an internal control
918 for normalization.
919
920 **Fig 3. *Pha21* is involved in virus accumulation.** (A) qRT-PCR was performed to
921 quantify the CymMV accumulation level and RNA level of *Pha21* in healthy (Mock)
922 and CymMV-infected (Cy-infected) *P. aphrodite.* The RNA level in the CymMV-
923 infected (Cy-infected) *P. aphrodite* was set to 1. Data represent mean ± SD; n = 3
924 biological replicates; **, $P < 0.01$; *, $P < 0.05$, Student's t test compared to mock. (B
925 and C) Transient silencing or overexpression of *Pha21* in CymMV-infected plants. qRT-

926 PCR was performed to quantify the RNA level of *Pha21* and CymMV accumulation
927 level from leaves of CymMV-infected *P. aphrodite* infiltrated with agrobacterium
928 carrying vector (Vector); hairpin RNA (hpRNA) vector to knockdown *Pha21*
929 (hpPha21-1 and hpPha21-2; B); or overexpression vector of *Pha21* (Pha21-oe; C). The
930 RNA level of plants infiltrated with control vector was set to 1. Data represent mean ±
931 SD; n = 3 biological replicates; **, $P < 0.01$; *, $P < 0.05$, Student's t test compared to
932 Vector. (D) The wild-type (WT) *P. equestris* orchid and transgenic *P. equestris*
933 (Pha21#8 and #9) were used for analysis. RNA level of *Pha21* and CymMV were
934 analyzed by qRT-PCR from leaves of WT or transgenic *P. equestris* (Pha21#8 and #9)
935 inoculated with CymMV. The RNA level of WT was set to 1. Data represent mean ±
936 SD; n = 2 biological replicates; **, $P < 0.01$; *, $P < 0.05$, Student's t-test compared to
937 WT. (A-D) *PhaUbiquitin 10* was used as an internal control for normalization.
938
939 **Fig 4. Overexpression of *Pha21* in engineered transgenic *Arabidopsis* enhances**
940 **resistance against viruses.** (A) Expression level of *Pha21* and accumulation level of
941 *Cucumber mosaic virus* (CMV) were analyzed by qRT-PCR from leaves of WT (Col-
942 0) or transgenic *Arabidopsis* (At-Pha21#4, #5, and #6). Data represent mean ± SD; n =
943 5 biological replicates; **, $P < 0.01$; *, $P < 0.05$, Student's t-test compared to WT.
944 *AtActin* was used as an internal control for normalization. (B) Disease symptoms of WT
945 (Col-0) or transgenic *Arabidopsis* (At-Pha21#4, #5, and #6) inoculated with CMV at
946 14 dpi. Images are one representative plant from five replicates; Scale bar, 1 cm.
947

948 **Fig 5. Pha21 confers self-ubiquitination E3 ligase activity and ubiquitin binding**
949 **ability.** (A) The *in vitro* self-ubiquitination E3 ligase activity assay was conducted on
950 wild-type Pha21, A20 mutant (Pha21-A20m), AN1 mutant (Pha21-AN1m), A20/AN1
951 double mutant (Pha21-A20mAN1m) with or without FLAG-Ub, human ubiquitin-
952 activating enzyme (hE1), or human ubiquitin-conjugating enzyme (hE2). Coomassie
953 staining for Pha21 was used as a loading control. Ubiquitinated proteins were analyzed
954 with immunoblotting using anti-FLAG antibodies. The ubiquitinated Pha21 are
955 indicted as Pha21-Ub. E1 conjugated with one Ub (E1-Ub), E2 conjugated with one or
956 two Ub (E2-Ub, E2-2Ub), and free Ub are indicated with a black arrow. (B) Yeast two-
957 hybrid assay was performed to analyze the interaction between full-length and deletion
958 mutant of Pha21 and ubiquitin. The schematic representations of full-length and
959 deletion mutant of Pha21 are indicated. The open rectangle indicates the entire Pha21
960 protein. A20 domain and AN1 domain are indicated as a dark blue oval circle and a
961 light blue oval circle, respectively. The full-length and deletion mutant of Pha21 cloned
962 in pGBKT7 vector were co-transformed with pGADT7-PhaUBQ into yeast AH109
963 strain. The 2DO indicates the Leucine and Trptophan dropout selective medium and
964 3DO indicates the Leucine, Trptophan, and Histidine dropout selective medium. The
965 pGBKT7 was used as a negative control.
966
967 **Fig 6. *Pha21* is involved in the expression of PhaNPR1-dependent gene, *PhaRdR1,***
968 **and PhaNPR1-independent gene, *PhaGRXC9*.** The expression levels of *Pha21,*
969 *PhaRdR1*, and *PhaGRXC9* were analyzed by qRT-PCR from leaves of *P. aphrodite*
970 infiltrated with agrobacterium carrying control vector (Vector) or hairpin RNA (hpRNA)

971 vector to knockdown *Pha21* (hpPha21-2; A), or to overexpress *Pha21* (Pha21-oe; B).
972 The RNA level of plants infiltrated with control vector was set to 1. Data represent
973 mean ± SD; n = 3 biological replicates; **, $P < 0.01$; *, $P < 0.05$, Student's t-test
974 compared to Vector. (A-B) *PhaUbiquitin 10* was used as an internal control for
975 normalization.
976
977 **Fig 7. *Pha21*, but not *Pha13*, is involved in the expression of *PhaDCL4* and**
978 ***PhaAGO1*.** The expression levels of *Pha13*, *Pha21*, *PhaRdR2*, *PhaRdR6*, *PhaDCL2*,
979 *PhaDCL4*, *PhaAGO1*, and *PhaAGO10* were analyzed by qRT-PCR from leaves of *P.*
980 *aphrodite* infiltrated with agrobacterium carrying control vector (Vector) or to
981 overexpress *Pha21* (Pha21-oe; A) or to overexpress *Pha13* (Pha13-oe; B). The RNA
982 level of plants infiltrated with control vector was set to 1. Data represent mean ± SD; n
983 = 3 biological replicates; **, $P < 0.01$; *, $P < 0.05$, Student's t-test compared to Vector.
984 (A-B) *PhaUbiquitin* 10 was used as an internal control for normalization.
985
986 **Fig 8. *AtSAP5* is involved in the expression of *DCL4* and *AGO1*.** The expression
987 levels of *AtSAP5, DCL4, AGO1* were analyzed by qRT-PCR in WT, AtSAP5
988 overexpression (AtSAP5-oe-4 and AtSAP5-oe-11) and RNAi lines (AtSAP5-RNAi-3
989 and AtSAP5-RNAi-7). Data represent mean ± SD; n = 5 biological replicates; **, $P <$
990 0.01; *, $P < 0.05$, Student's t-test. Student's t test compared to WT. *AtActin* was used
991 as an internal control for normalization.
992

993 **Fig 9. Pha21 A20 and AN1 domain play different roles in the expression of**
994 ***PhaDCL4, PhaAGO1, PhaGRXC9* and virus resistance.**
995 The expression level of *Pha21*, *PhaDCL4, PhaAGO1*, *PhaGRXC9* and CymMV
996 accumulation level were analyzed by qRT-PCR in leaves of healthy *P. aphrodite* (A),
997 or CymMV pre-infected *P. aphrodite* (B) infiltrated with agrobacterium carrying
998 control vector (Vector), overexpression clones of Pha21 (Pha21-oe), or the respective
999 A20 and/or AN1 mutant clones (Pha21A20m, Pha21AN1m, and Pha21A20mAN1m).
1000 The RNA level of plants infiltrated with control vector was set to 1. Data represent
1001 mean ± SD; n = 3 biological replicates; **, $P < 0.01$; *, $P < 0.05$; ns, no significant
1002 difference, Student's t test compared to Vector. (A-B) *PhaUbiquitin 10* was used as an
1003 internal control for normalization.
1004
1005 **Fig 10. The role of A20/AN1 proteins in antiviral immunity.**
1006 A model illustrating the roles of SA-induced-A20/AN1 proteins Pha13 and Pha21 from
1007 *Phalaenopsis aphrodite,* and AtSAP5 from *Arabidopsis thaliana* in antiviral immunity.
1008 Virus infection caused accumulation of SA and led to the activation of *Pha13*, *Pha21*,
1009 and *AtSAP5*, allowing it to trigger the SA-and RNAi-mediated immune responsive
1010 genes including *NPR1*, *GRXC9*, *DCL4*, *AGO1*, and *RdR1* in antiviral immunity.
1011
1012

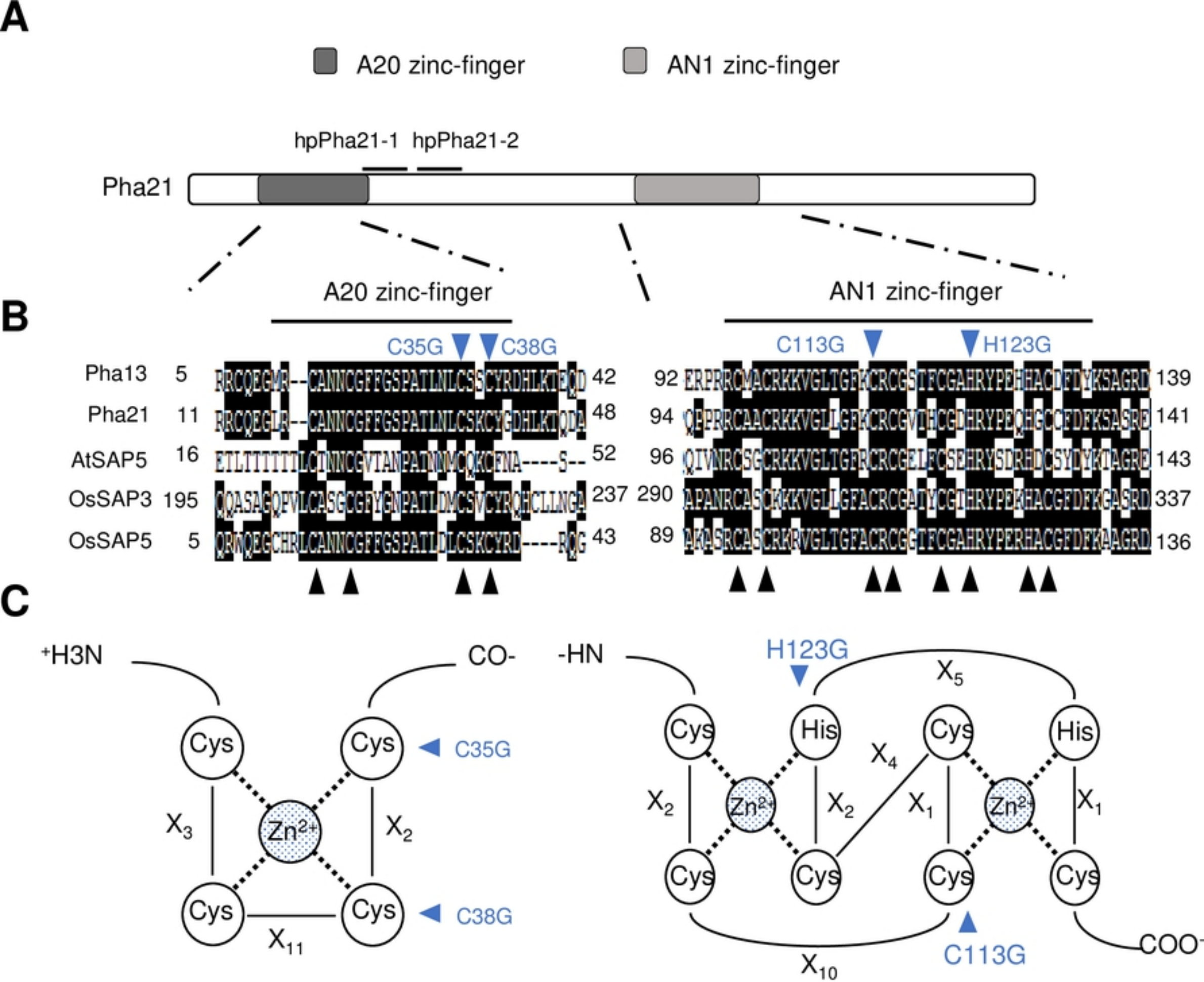
A
A20 zinc-finger
AN1 zinc-finger
hpPha21-1
hpPha21-2
Pha21
B
A20 zinc-finger
AN1 zinc-finger
C35G
C38G
C113G
H123G
Pha13
Pha21
AtSAP5
OsSAP3
OsSAP5
C
+H3N
CO-
-HN
COO-
Cys
His
Zn2+
X1
X2
X3
X4
X5
X10
X11
C35G
C38G
H123G
C113G

Fig 1

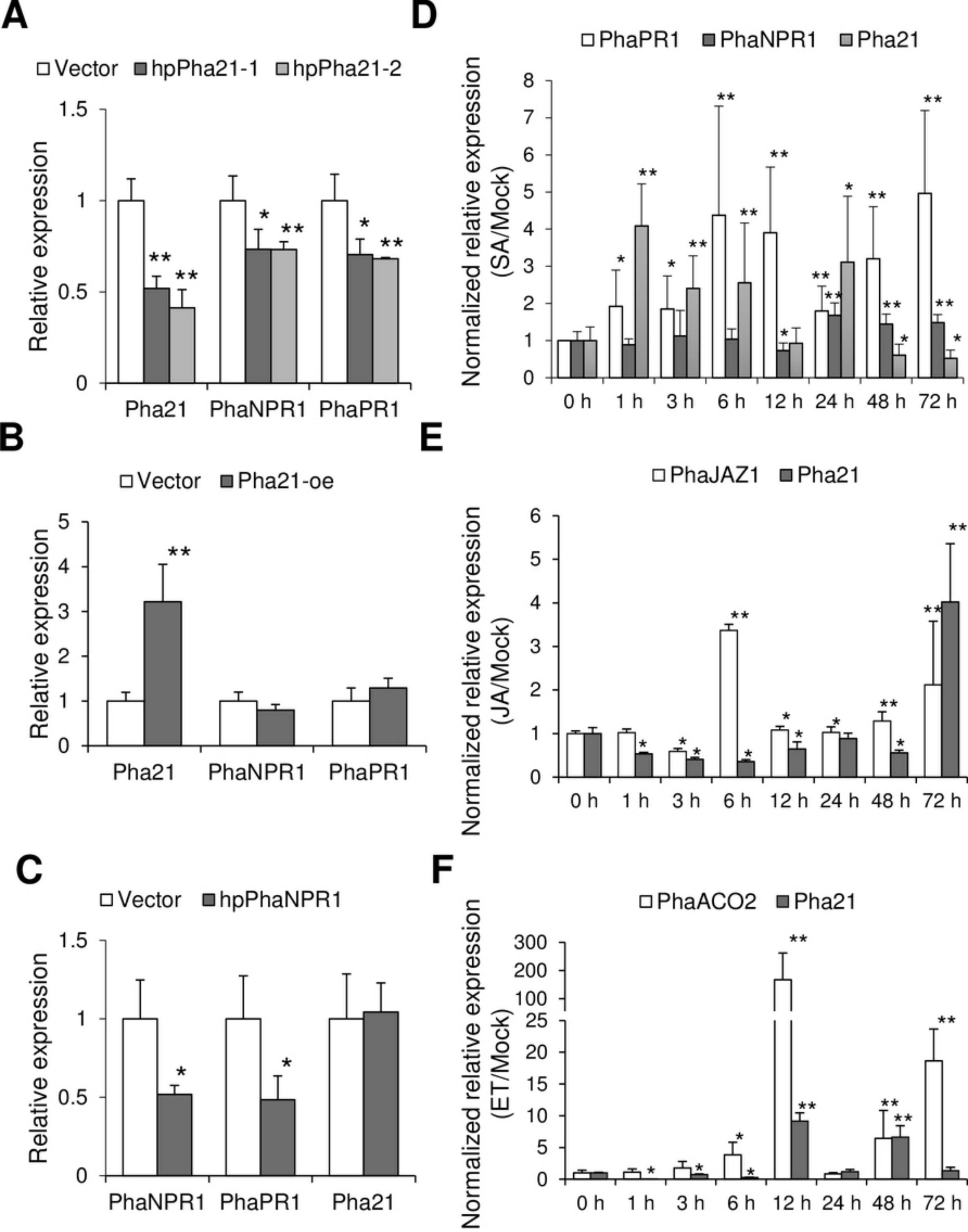
A
Vector
hpPha21-1
hpPha21-2
Relative expression
Pha21
PhaNPR1
PhaPR1
B
Vector
Pha21-oe
Relative expression
Pha21
PhaNPR1
PhaPR1
C
Vector
hpPhaNPR1
Relative expression
PhaNPR1
PhaPR1
Pha21
D
PhaPR1
PhaNPR1
Pha21
Normalized relative expression (SA/Mock)
0 h
1 h
3 h
6 h
12 h
24 h
48 h
72 h
E
PhaJAZ1
Pha21
Normalized relative expression (JA/Mock)
0 h
1 h
3 h
6 h
12 h
24 h
48 h
72 h
F
PhaACO2
Pha21
Normalized relative expression (ET/Mock)
0 h
1 h
3 h
6 h
12 h
24 h
48 h
72 h

Fig 2

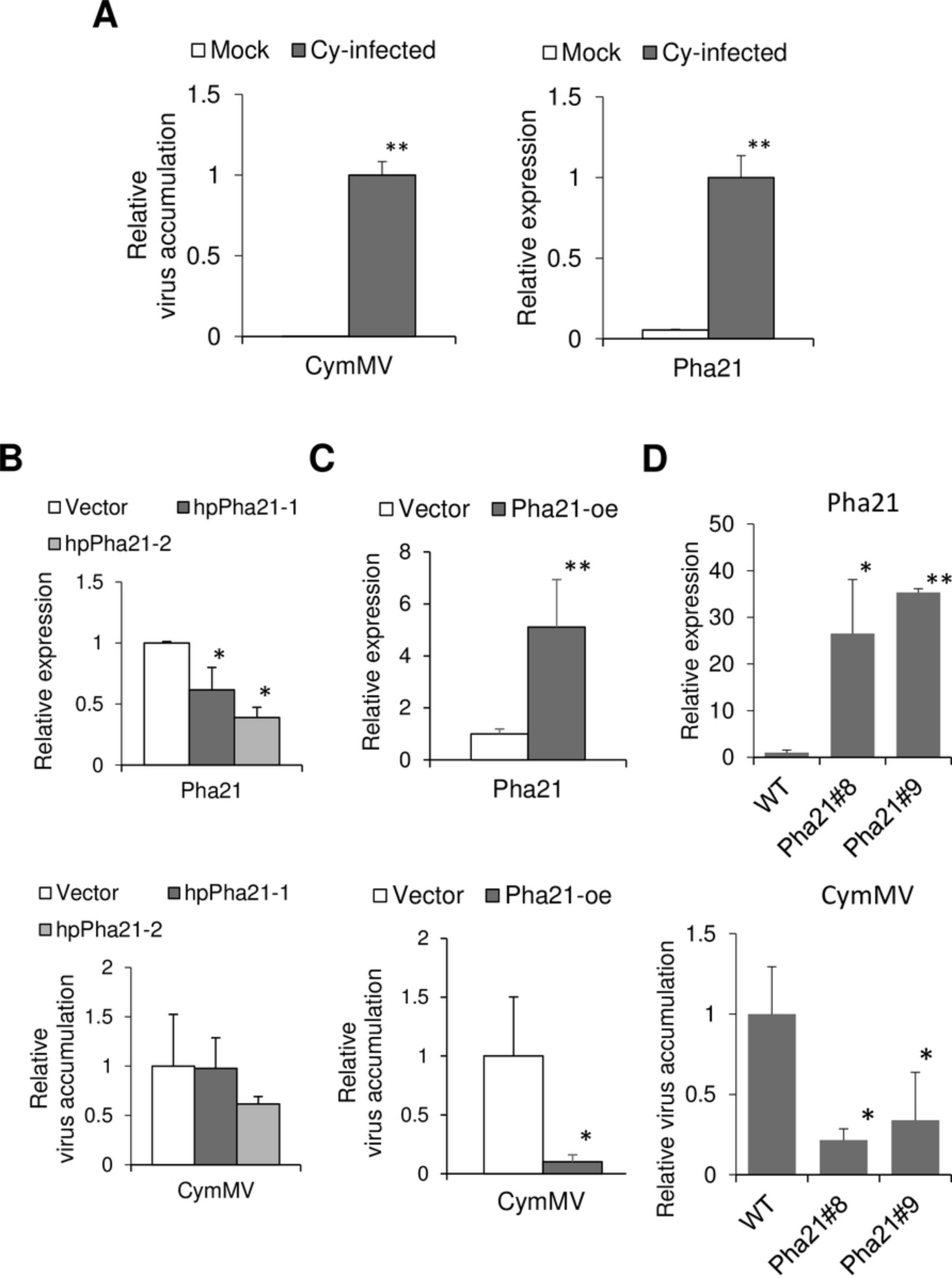
A
Mock
Cy-infected
Relative virus accumulation
1.5
1
0.5
0
**
CymMV
Mock
Cy-infected
Relative expression
1.5
1
0.5
0
**
Pha21
B
Vector
hpPha21-1
hpPha21-2
Relative expression
1.5
1
0.5
0
*
*
Pha21
Vector
hpPha21-1
hpPha21-2
Relative virus accumulation
2
1.5
1
0.5
0
CymMV
C
Vector
Pha21-oe
Relative expression
8
6
4
2
0
**
Pha21
Vector
Pha21-oe
Relative virus accumulation
2
1.5
1
0.5
0
*
CymMV
D
Pha21
Relative expression
50
40
30
20
10
0
*
**
WT
Pha21#8
Pha21#9
CymMV
Relative virus accumulation
1.5
1
0.5
0
*
*
WT
Pha21#8
Pha21#9

Fig 3

A

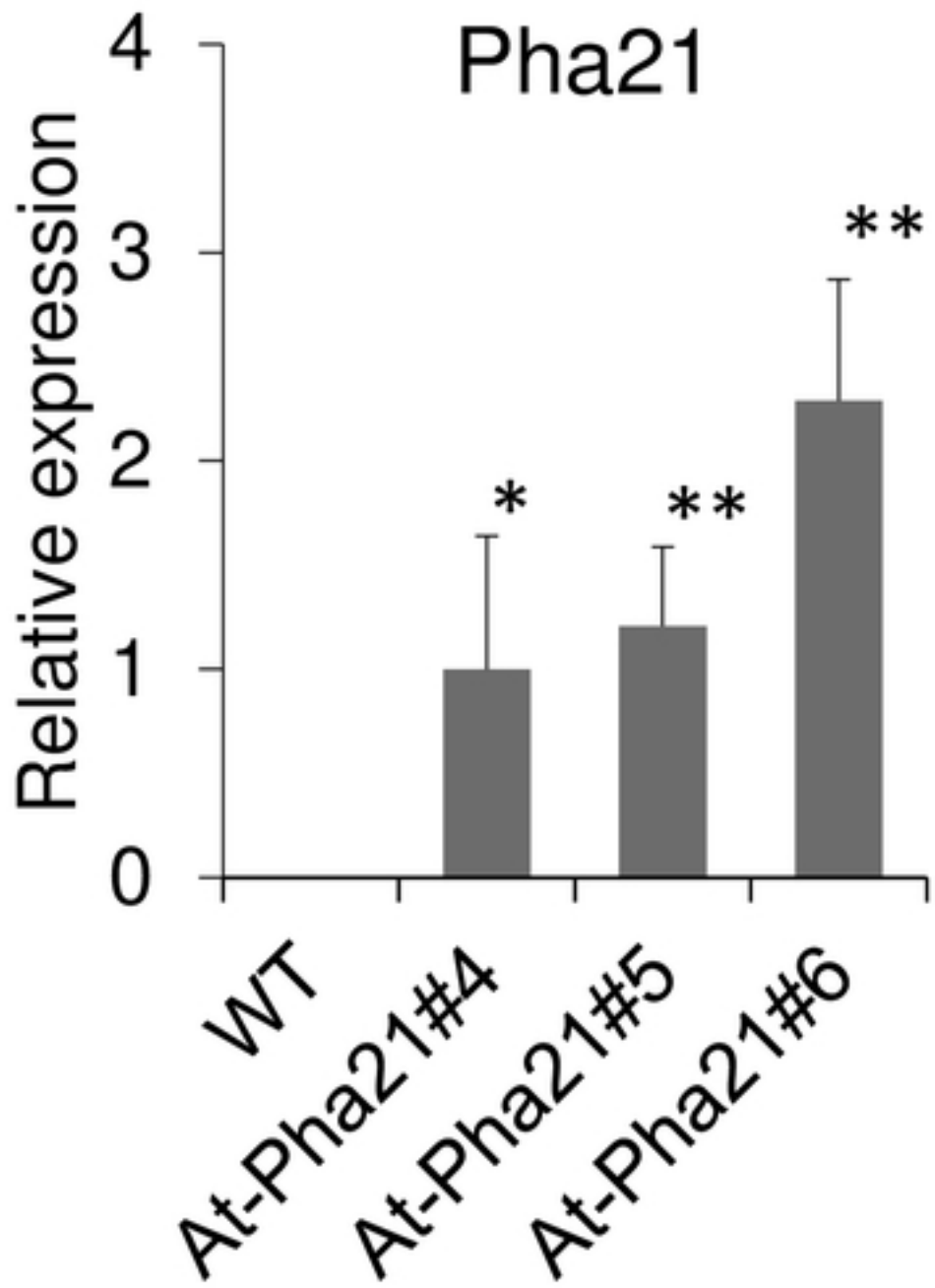
Pha21
Relative expression
4
3
2
1
0
*
**
**
WT
At-Pha21#4
At-Pha21#5
At-Pha21#6

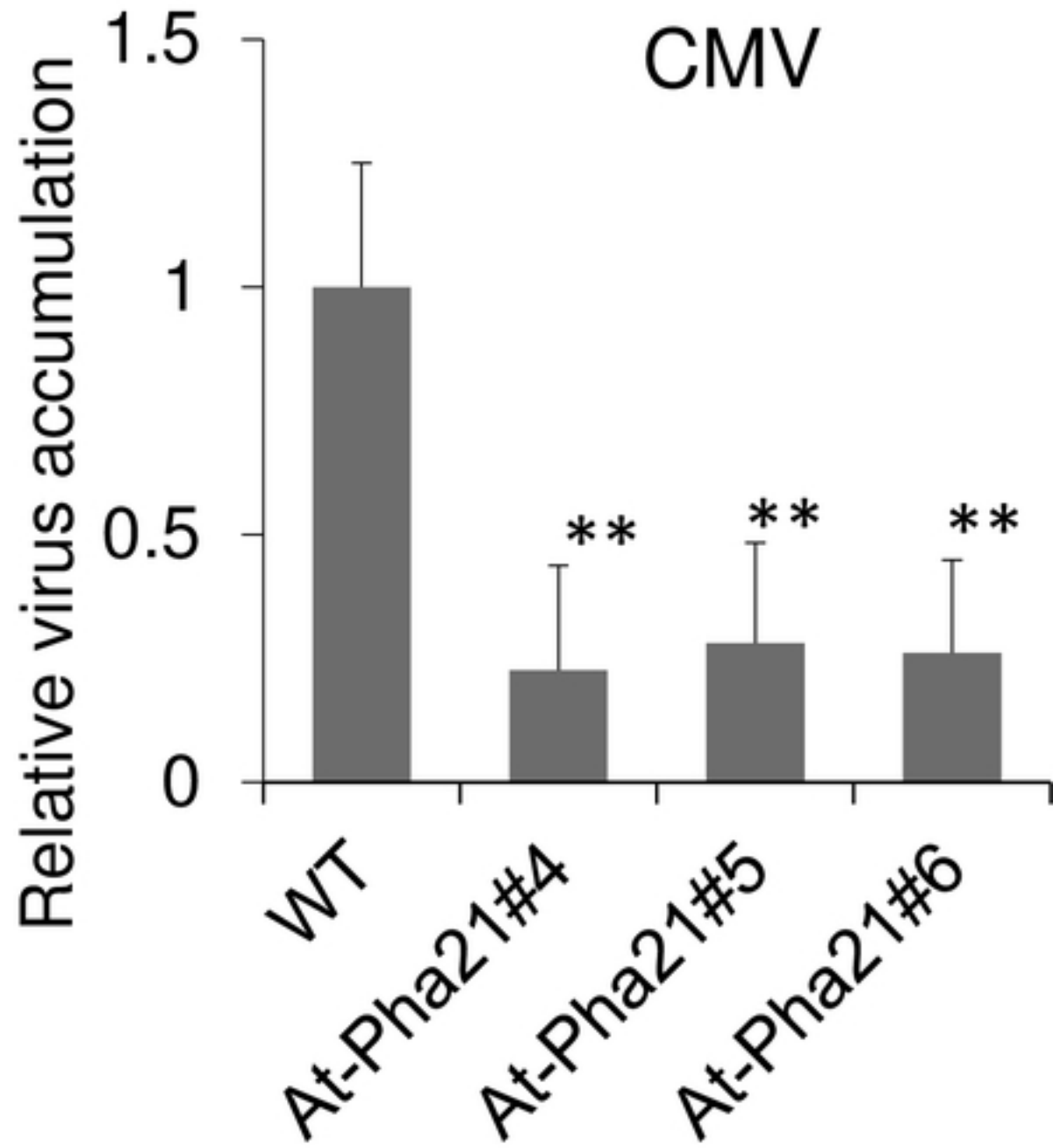
CMV
Relative virus accumulation
1.5
1
0.5
0
**
**
**
WT
At-Pha21#4
At-Pha21#5
At-Pha21#6

B

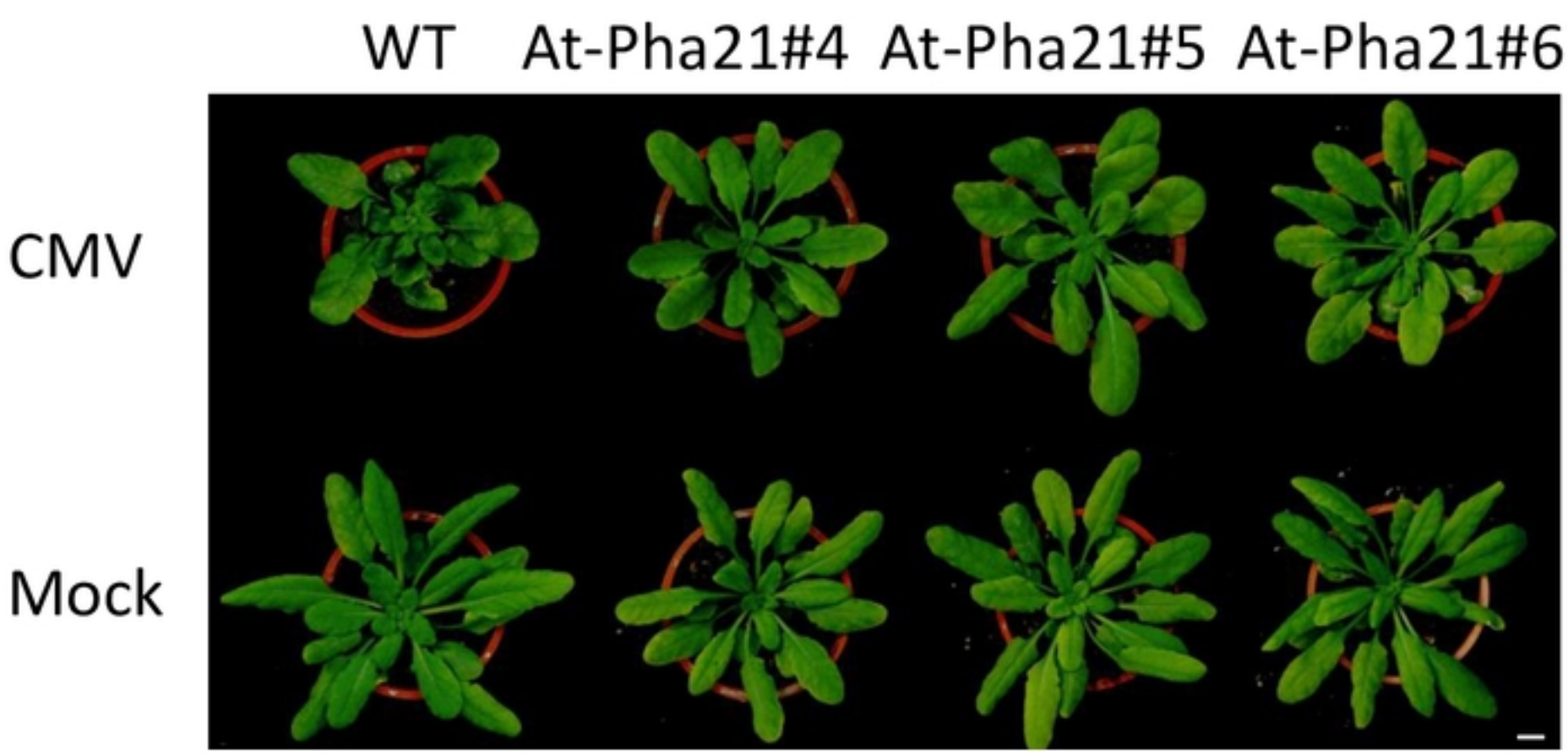
WT
At-Pha21#4
At-Pha21#5
At-Pha21#6
CMV
Mock

Fig 4

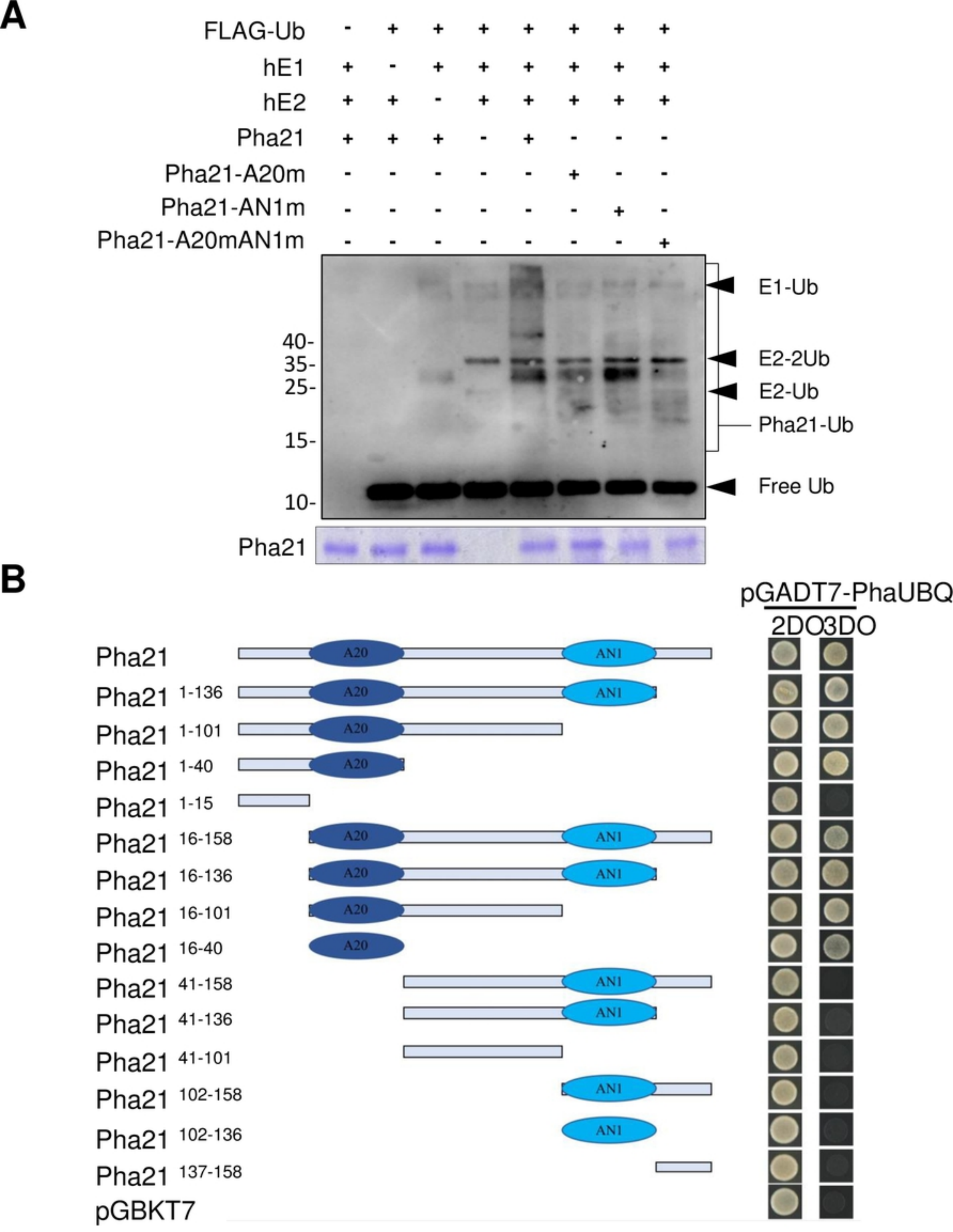
A
FLAG-Ub
hE1
hE2
Pha21
Pha21-A20m
Pha21-AN1m
Pha21-A20mAN1m
40-
35-
25-
15-
10-
E1-Ub
E2-2Ub
E2-Ub
Pha21-Ub
Free Ub
Pha21
B
pGADT7-PhaUBQ
2DO
3DO
Pha21
Pha21 1-136
Pha21 1-101
Pha21 1-40
Pha21 1-15
Pha21 16-158
Pha21 16-136
Pha21 16-101
Pha21 16-40
Pha21 41-158
Pha21 41-136
Pha21 41-101
Pha21 102-158
Pha21 102-136
Pha21 137-158
pGBKT7
A20
AN1

Fig 5

A

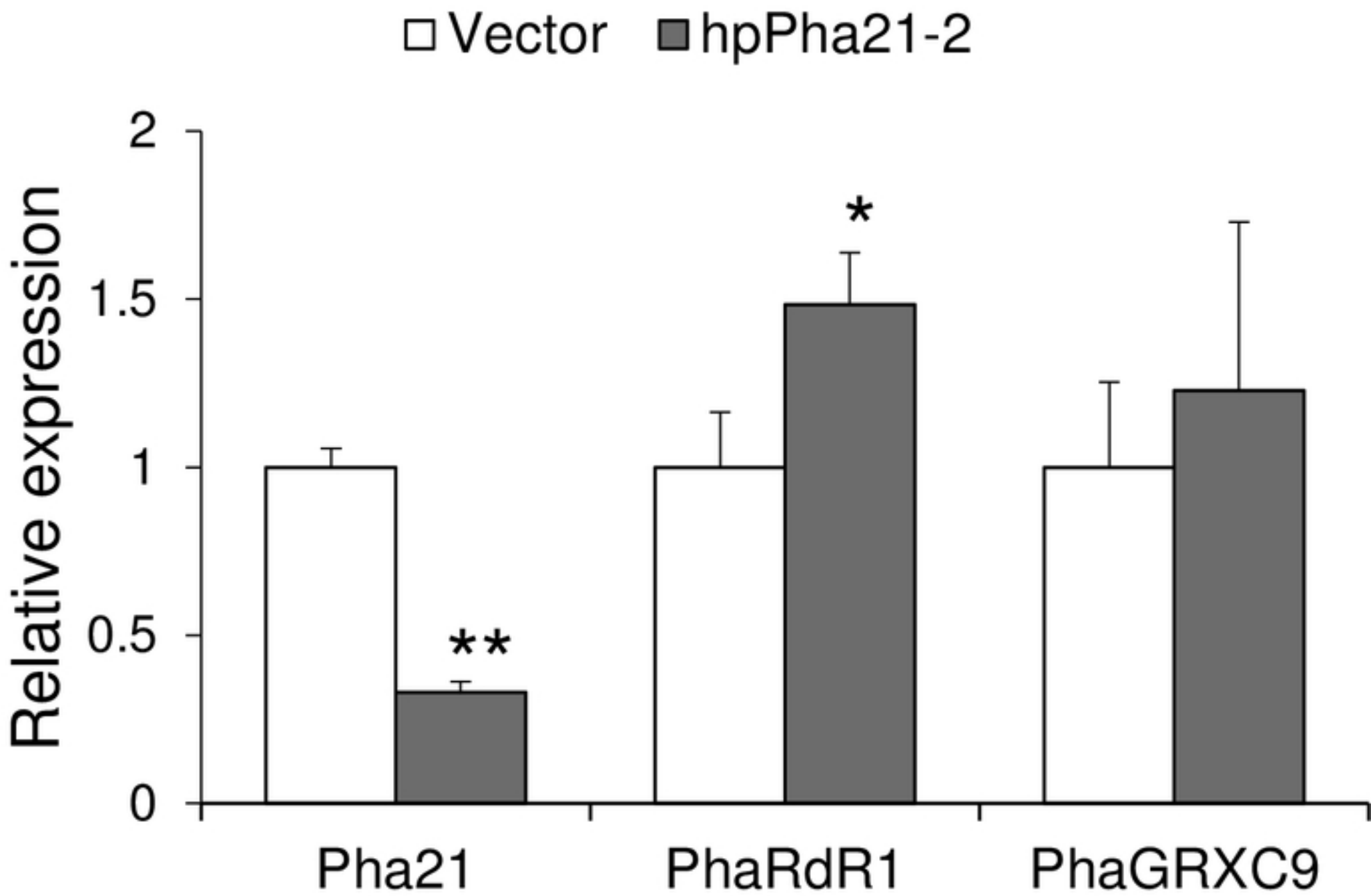
Vector
hpPha21-2
Relative expression
2
1.5
1
0.5
0
**
*
Pha21
PhaRdR1
PhaGRXC9

B

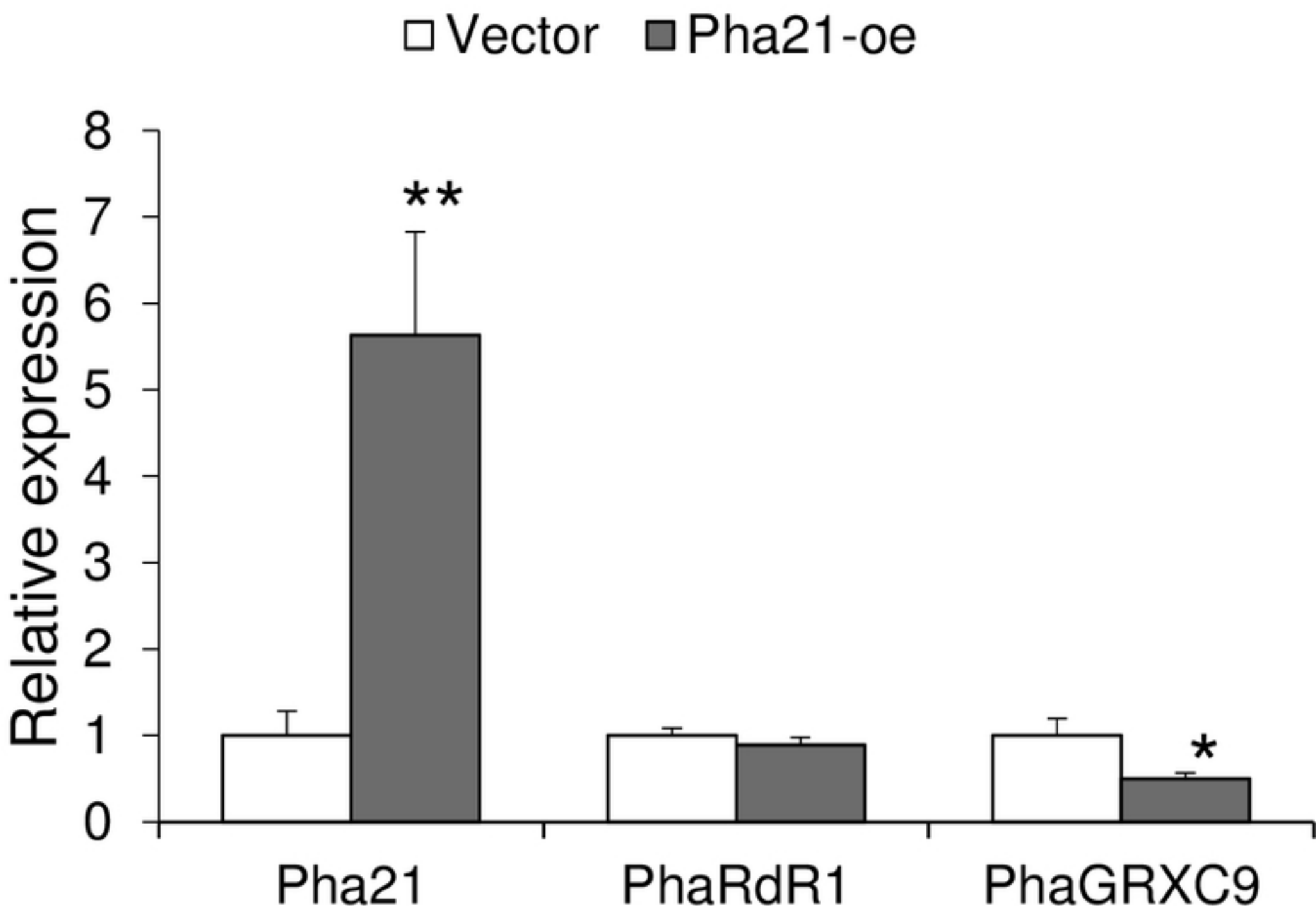
Vector
Pha21-oe
Relative expression
8
7
6
5
4
3
2
1
0
**
*
Pha21
PhaRdR1
PhaGRXC9

Fig 6

A

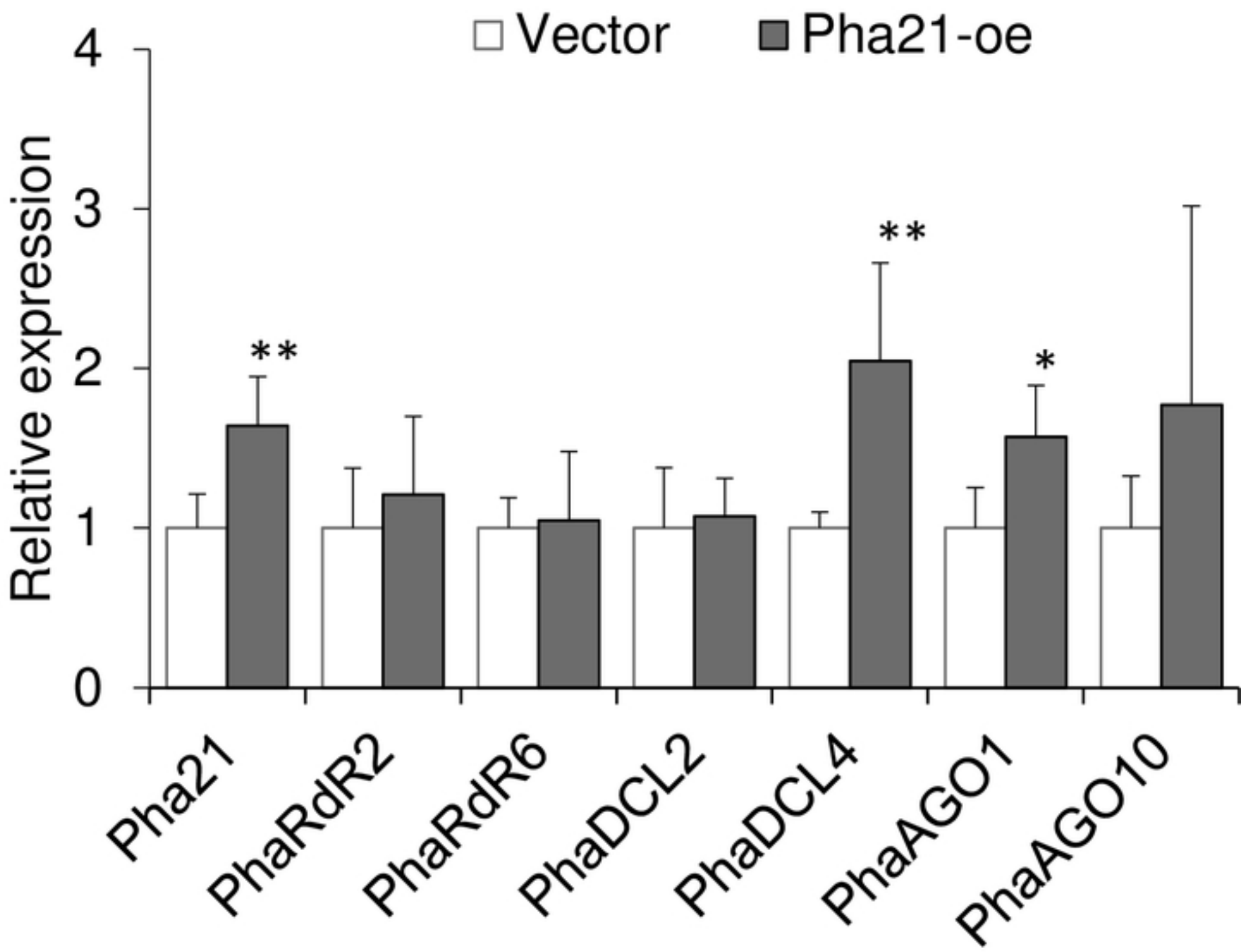
Vector
Pha21-oe
Relative expression
0
1
2
3
4
**
**
*
Pha21
PhaRdR2
PhaRdR6
PhaDCL2
PhaDCL4
PhaAGO1
PhaAGO10

B

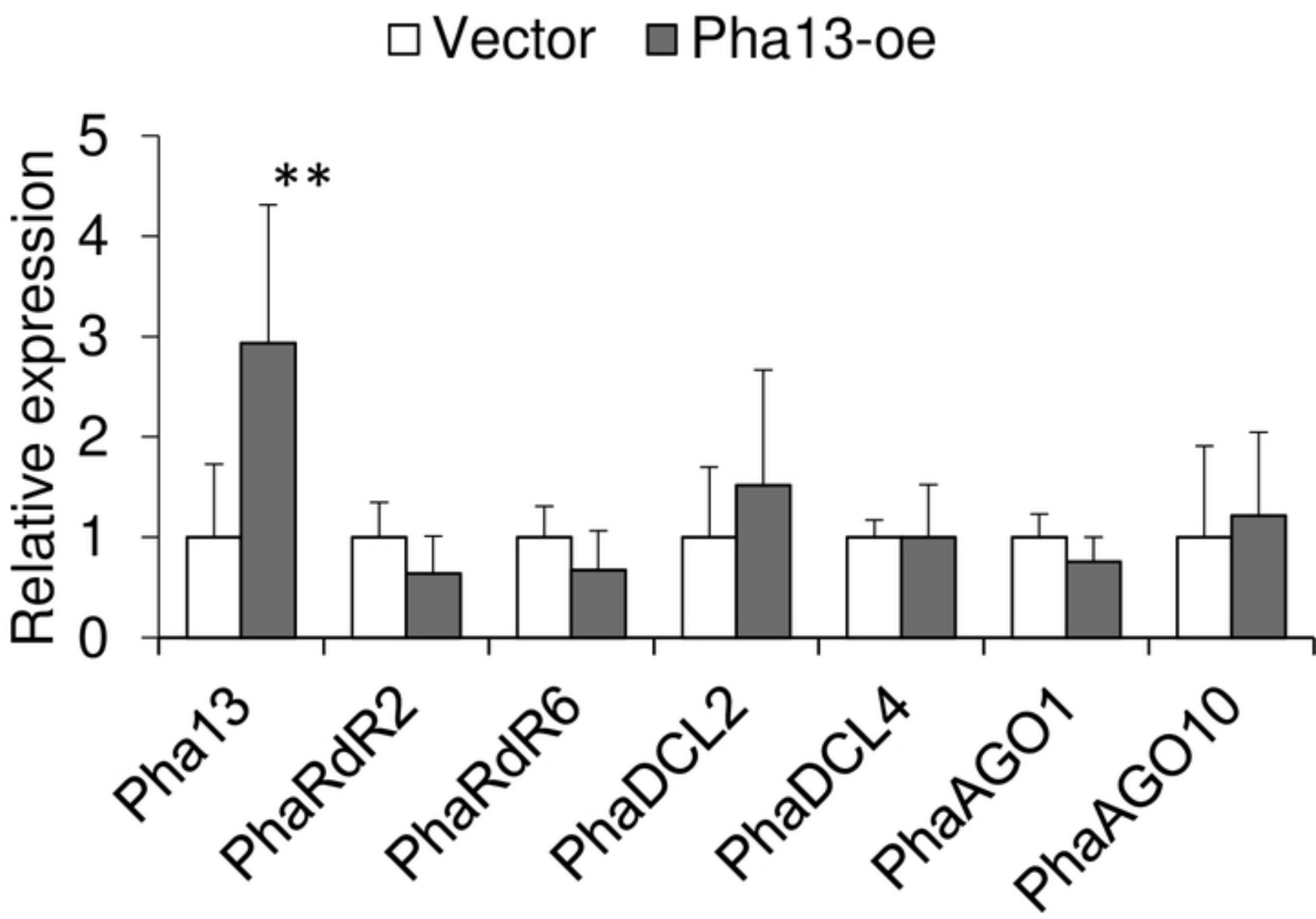
Vector
Pha13-oe
Relative expression
0
1
2
3
4
5
**
Pha13
PhaRdR2
PhaRdR6
PhaDCL2
PhaDCL4
PhaAGO1
PhaAGO10

Fig 7

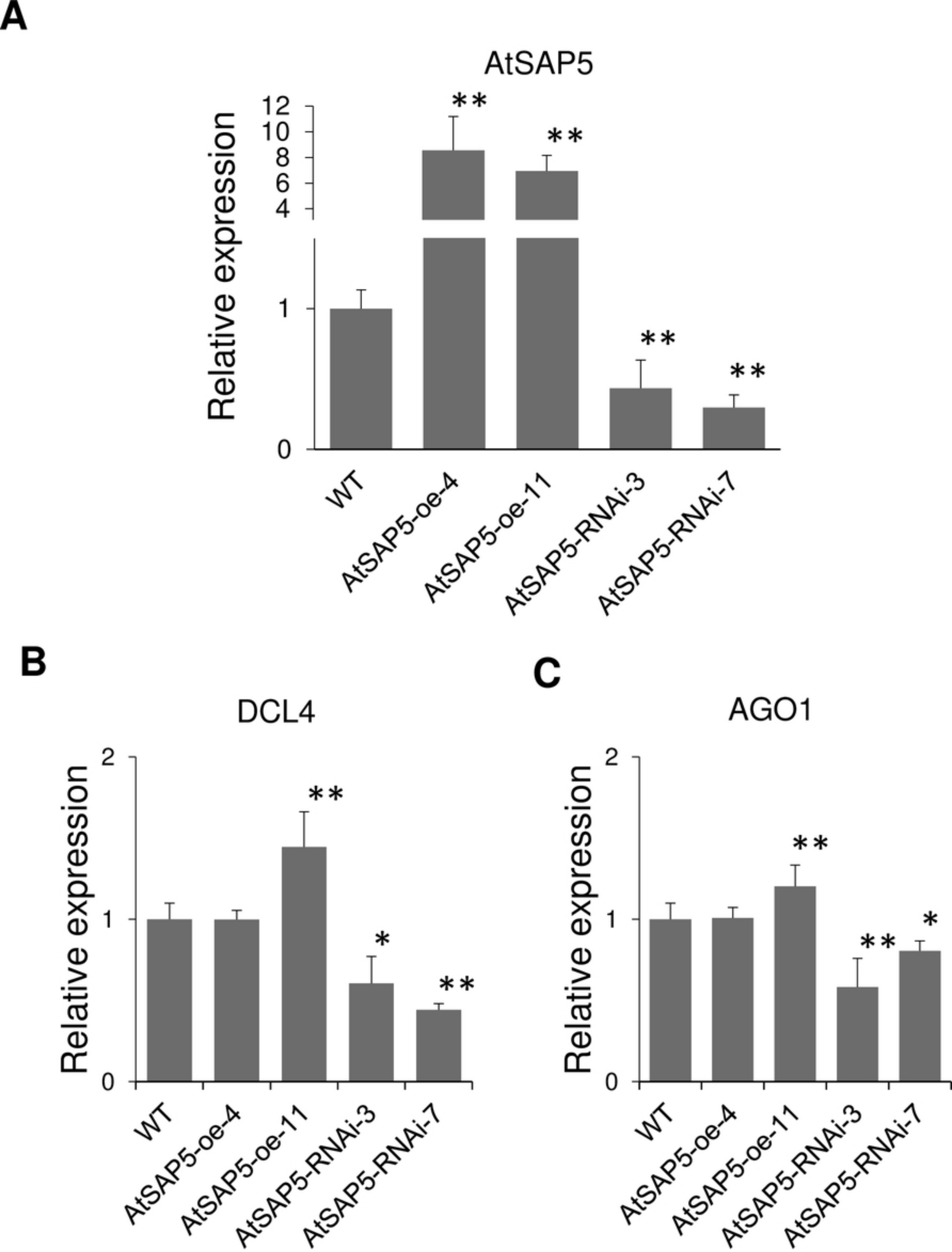
A
AtSAP5
Relative expression
12
10
8
6
4
1
0
**
**
**
**
WT
AtSAP5-oe-4
AtSAP5-oe-11
AtSAP5-RNAi-3
AtSAP5-RNAi-7
B
DCL4
Relative expression
2
1
0
**
*
**
WT
AtSAP5-oe-4
AtSAP5-oe-11
AtSAP5-RNAi-3
AtSAP5-RNAi-7
C
AGO1
Relative expression
2
1
0
**
**
*
WT
AtSAP5-oe-4
AtSAP5-oe-11
AtSAP5-RNAi-3
AtSAP5-RNAi-7

Fig 8

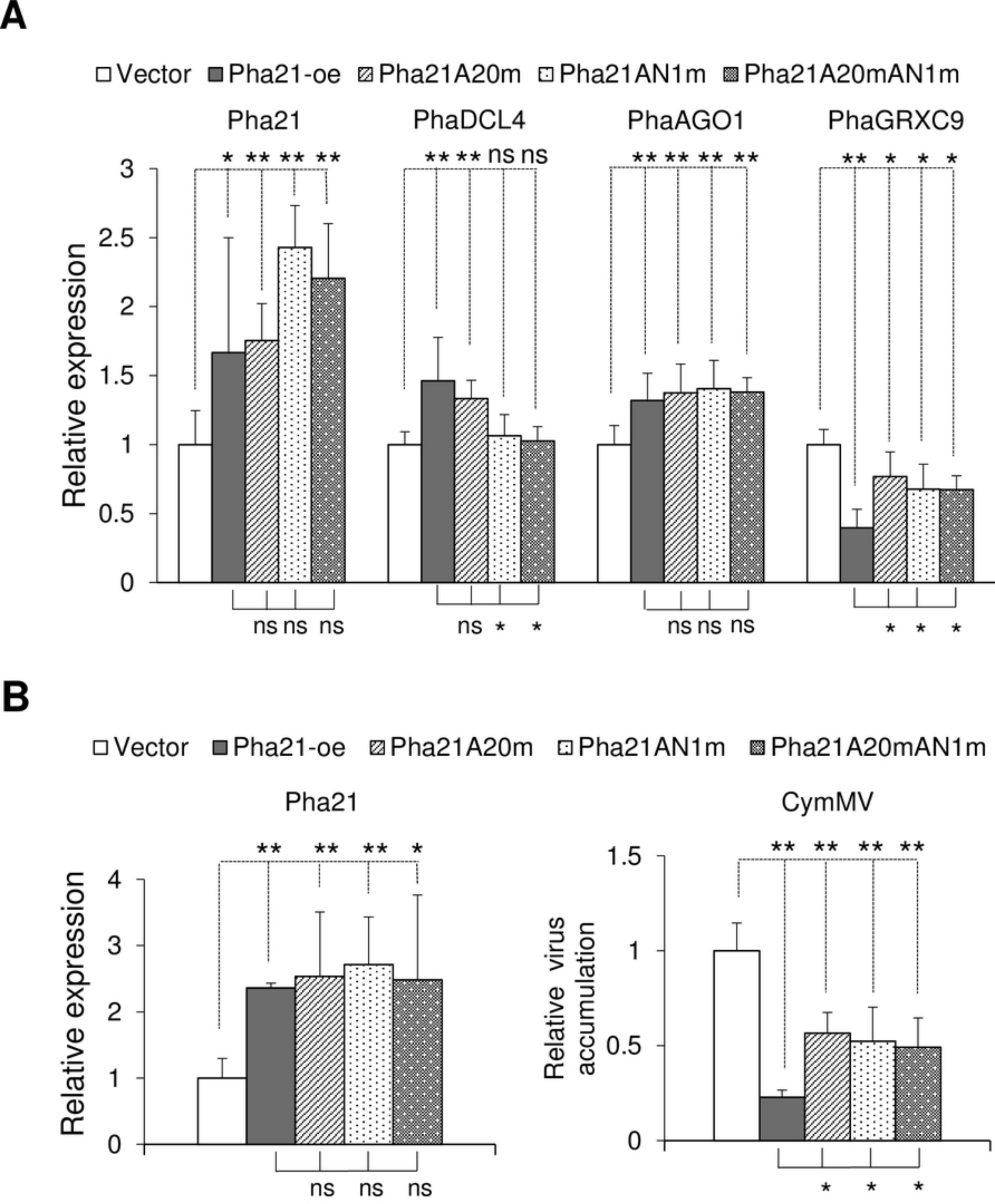
A
Vector
Pha21-oe
Pha21A20m
Pha21AN1m
Pha21A20mAN1m
Pha21
PhaDCL4
PhaAGO1
PhaGRXC9
Relative expression
3
2.5
2
1.5
1
0.5
0
* ** ** **
** ** ns ns
** ** ** **
** * * *
ns ns ns
ns * *
ns ns ns
* * *
B
Vector
Pha21-oe
Pha21A20m
Pha21AN1m
Pha21A20mAN1m
Pha21
CymMV
Relative expression
4
3
2
1
0
** ** ** *
ns ns ns
Relative virus accumulation
1.5
1
0.5
0
** ** ** **
* * *

Fig 9

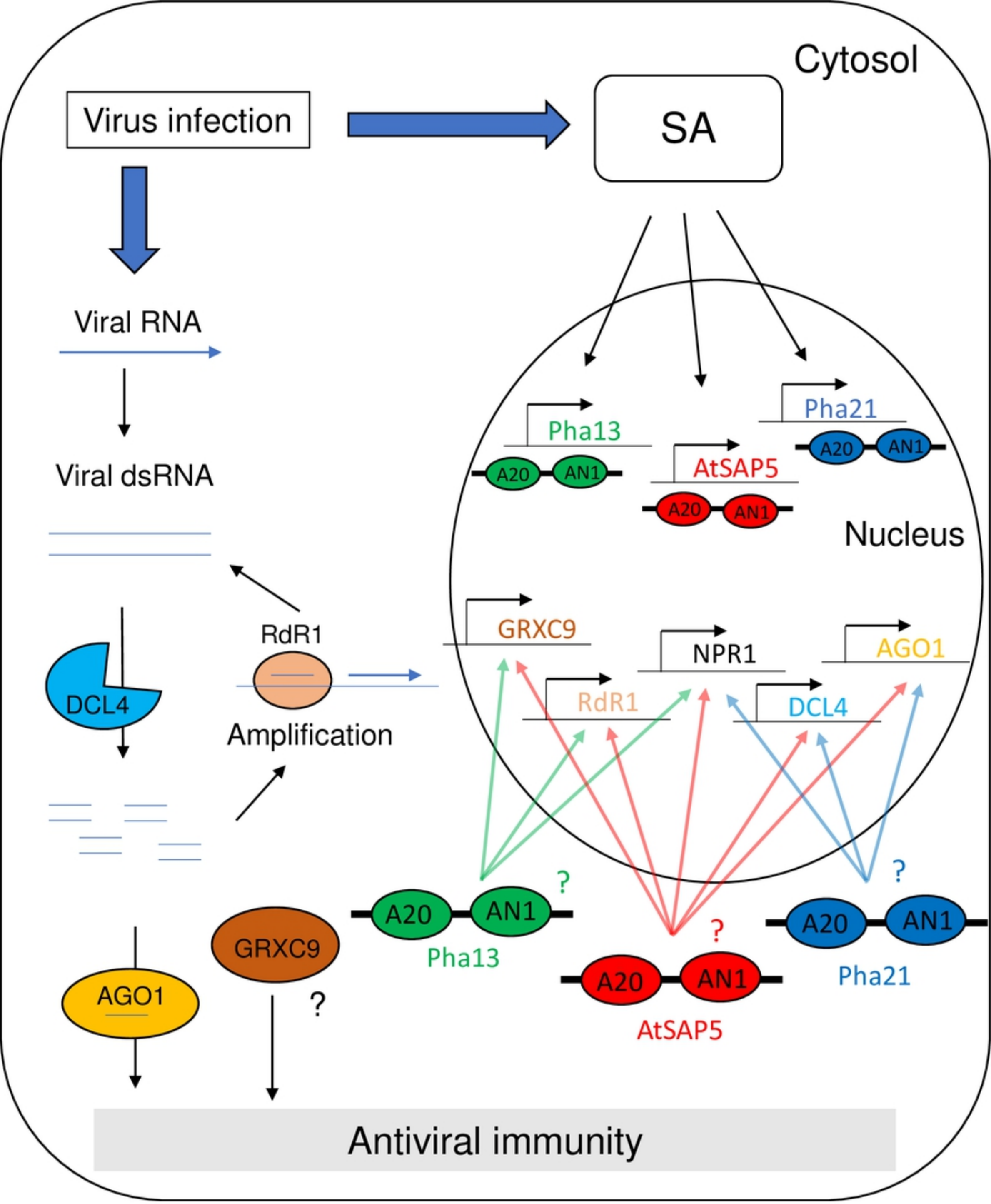
Cytosol
Virus infection
SA
Viral RNA
Viral dsRNA
Pha21
Pha13
A20
AN1
AtSAP5
Nucleus
GRXC9
NPR1
AGO1
RdR1
DCL4
Amplification
?
AGO1
GRXC9
Pha13
Pha21
AtSAP5
Antiviral immunity

Fig 10